BMO-TR-91-03
QUEST TR-508

AD-A234 628

Abrasive-Waterjet Machining Of Isogrid Structures

Mohamed Hashish
Mark Marvin
David Monserud

QUEST Integrated, Inc.
21414 - 68th Avenue South
Kent, Washington 98032
(206) 872-9500

DTIC
APR 2 1991
C

Revised
December 1990

Prepared for

Ballistic Missile Organization/SSD
Norton Air Force Base, California 92409-6468

91 4 11 031

This report was submitted by Quest Integrated Inc., 21414 68th Avenue South, Kent, Washington 98032, under contract F04704-90-C-0033. This effort was accomplished in support of the Phase I SBIR program at the Ballistic Missile Organization (AFSC), Norton AFB, CA 92409-6468. This report has been reviewed and approved for publication.

Wayne B. Osborn GS-11
Manufacturing Staff Engineer

Timothy M. Jenkins GM-13
Acting Director of Manufacturing
and Quality Assurance

1. AGENCY USE ONLY (Leave blank)	2. REPORT DATE 18 Dec 90	3. REPORT TYPE AND DATES COVERED Final, 14 May 90–13 Nov 90	

4. TITLE AND SUBTITLE	5. FUNDING NUMBERS
Abrasive-Waterjet Machining of Isogrid Structures	F04704-90-C-0033

6. AUTHOR(S)

Mohamed Hashish, Mark Marvin, David Monserud

7. PERFORMING ORGANIZATION NAME(S) AND ADDRESS(ES) Quest Integrated, Inc. 21414 – 68th Avenue South Kent, WA 98032	8. PERFORMING ORGANIZATION REPORT NUMBER TR-508

9. SPONSORING/MONITORING AGENCY NAME(S) AND ADDRESS(ES) Ballistic Missile Organization Air Force Systems Command Norton AFB, CA 92409-6468	10. SPONSORING/MONITORING AGENCY REPORT NUMBER BMO-TR-91-03

11. SUPPLEMENTARY NOTES

12a. DISTRIBUTION/AVAILABILITY STATEMENT Approved for public release; distribution unlimited.	12b. DISTRIBUTION CODE

13. ABSTRACT (Maximum 200 words)

An experimental investigation was conducted to determine the feasibility of machining isogrid structures with abrasive-waterjets (AWJs). The main objective was to mill isogrid patterns in surfaces with accurate depth control using an AWJ. Three different approaches using AWJs were tested: linear cutting of isogrid patterns for diffusion bonding, milling with conventional AWJ nozzles, and milling with a single-angled rotary AWJ nozzle. It was shown that pocket milling with conventional AWJs is the most feasible of those tested. The milling can be done internally on preformed aluminum tubes, and the AWJ can also be used on materials other than aluminum. Accurate depth control can be achieved at high productivity rates. As an example, it is projected that a 48-inch-diameter skirt 12 inches high could be milled with an isogrid pattern in 6.3 hours. Milled isogrid patterns can be controlled to 0.001 inch, and thin walls of less than 0.025 inch are achievable. Milling isogrid patterns with conventional AWJs could be very economical, but additional development efforts are required to optimize the milling process and to demonstrate the milling of prototype parts.

14. SUBJECT TERMS Abrasive-waterjet, cutting, milling, drilling, machining, isogrid, diffusion bonding, aluminum			15. NUMBER OF PAGES 57
			16. PRICE CODE

17. SECURITY CLASSIFICATION OF REPORT unclassified	18. SECURITY CLASSIFICATION OF THIS PAGE unclassified	19. SECURITY CLASSIFICATION OF ABSTRACT unclassified	20. LIMITATION OF ABSTRACT unlimited

TABLE OF CONTENTS

LIST OF FIGURES

LIST OF TABLES

1. INTRODUCTION

This report describes the results of an experimental feasibility investigation of machining isogrid structures using abrasive-waterjet (AWJ) technology. The work was conducted as a Phase I SBIR (Small Business Innovation Research) program for the U.S Air Force by Quest Integrated, Inc., under contract number F04704-90C-0033.

Isogrids are lightweight structures with high strength-to-weight ratios. Figure 1 shows a section of a typical isogrid pattern for the propulsion skirt in a post-boost vehicle. Isogrids are used in small ICBMs and SSD's extendable launch vehicles. They have recently been dropped from the ICBM production program, however, because of high manufacturing costs. Current isogrid manufacturing processes are prohibitively expensive due to slow machining cycles and untenable scrap rates.

Milling is the current method used for machining the isogrid pattern. After a part is milled, it is then rolled into a cylindrical form. This process often results in distortions of the isogrid ribs. It is also expensive and time-consuming, and limited to certain isogrid geometries.

Abrasive-waterjets have proven to be very successful in many machining applications and offer an economical alternative for the machining of isogrid structures. The potential advantages of the AWJ technique for this application are:

- High productivity
- No residual stresses
- Integral machining capability
- Capability of machining a wide range of isogrid geometries and materials

The present experimental investigation was conducted to study novel concepts for machining isogrid structures using AWJs. The main manufacturing technique addressed was integral machining with an AWJ to mill cylindrical sections internally with the net isogrid pattern shape. Several other concepts were also investigated. Both the technical and economic feasibility of the AWJ method were evaluated.

In this report, background information about AWJ cutting is presented first in the following section. Then the Phase I objectives and technical approach are reviewed, followed by details of the experimental machining tests and the economic analysis. Conclusions are summarized and recommendations presented in the final section.
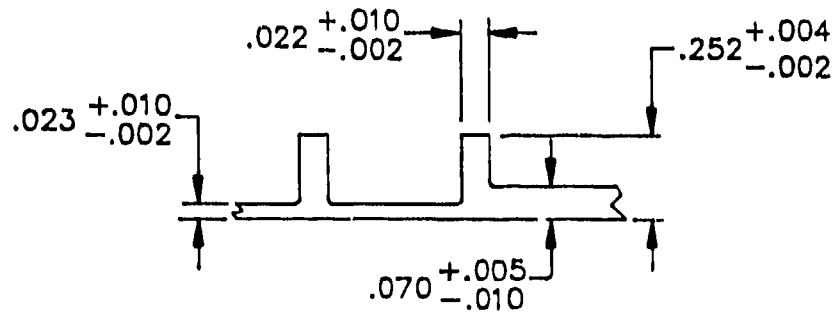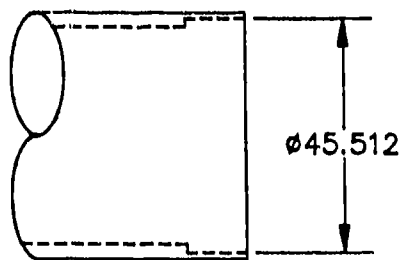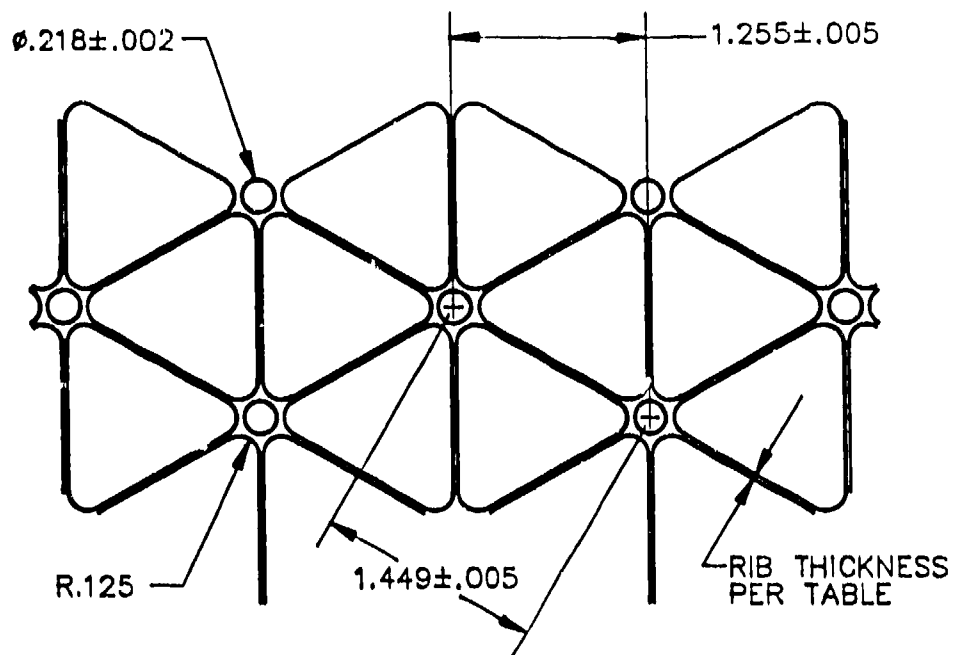
Figure 1. **Isogrid Geometry**

2. BACKGROUND INFORMATION

In this section, general background information on the AWJ technology is presented, along with a description of the single-angled rotary AWJ, an AWJ geometry that was tested in this study.

2.1 AWJ Nozzle and Parameters

Figure 2 shows a schematic of an AWJ nozzle and the most critical performance parameters. Water pressurized to 60 ksi enters the nozzle and is then expelled through a sapphire orifice to form a coherent high-velocity waterjet. Typical jet diameters are 0.006 to 0.030 inch, and typical jet velocities are 1500 to 3000 ft/sec. The flow of the high-velocity waterjet into the concentrically aligned mixing tube creates a vacuum, which is used to transport abrasives from a hopper to the nozzle abrasive chamber via a suction hose. A typical abrasive material is garnet, which has flow rates of up to 3 lb/min. Medium to fine sizes (mesh 60 to mesh 200) are most commonly used for metal, glass, and resin composites. Abrasives are accelerated and axially oriented (focused) in the mixing tube, which has a length-to-diameter ratio between 50 and 100. Typical tube diameters are 0.03 to 0.09 inch, with lengths up to 6 inches. As a result of momentum transfer between the water and the abrasives, a focused, high-velocity stream of particles (the AWJ) exits the nozzle and performs the cutting.

Two wear modes of erosion are involved in the AWJ material removal process: (1) the cutting wear mode, which is a micromachining process that occurs at shallow angles of impact, and (2) the deformation wear mode, which occurs at large angles of impact and results in material removal due to microcracking and plastic deformation. Observations of cut surfaces do not suggest any thermal modes of material removal. Because of the very localized erosion process of AWJs, there are no adverse mechanical effects associated with the cutting process, such as residual stress.

2.2 Current Performance of AWJs

Many materials can be cut with AWJs, including hard steels, titanium, aluminum, cast iron, high-strength composites, armor-layered glass, ceramics, rocks, and steel-reinforced concrete. Figure 3a shows a sample of laminated armor glass cut with an AWJ. AWJs have also been investigated for some machining operations, such as milling, turning, and piercing (Hashish, 1988). Figure 3b shows a sample of a milled shape in glass. Milling with an AWJ is accomplished by multipass traverses of the jet over the material. The material removal rate and surface textural features are controlled by varying the AWJ parameters. Figure 3c shows a magnesium boron carbide rod turned with an AWJ. One pass was used to produce a near-net

PARAMETERS

Waterjet Pressure
Waterjet Diameter

Abrasive Flow Rate
Abrasive Size
Abrasive Material

Mixing Length
Mixing Diameter

Traverse Speed
Angle of Cut
Stand Off Distance

Depth of Cut
Width of Cut
Waviness & Roughness

COMPONENTS

High Pressure Tube

Abrasive Feed Hose

Waterjet Orifice

Waterjet

Mixing Tube

Abrasive—Waterjet
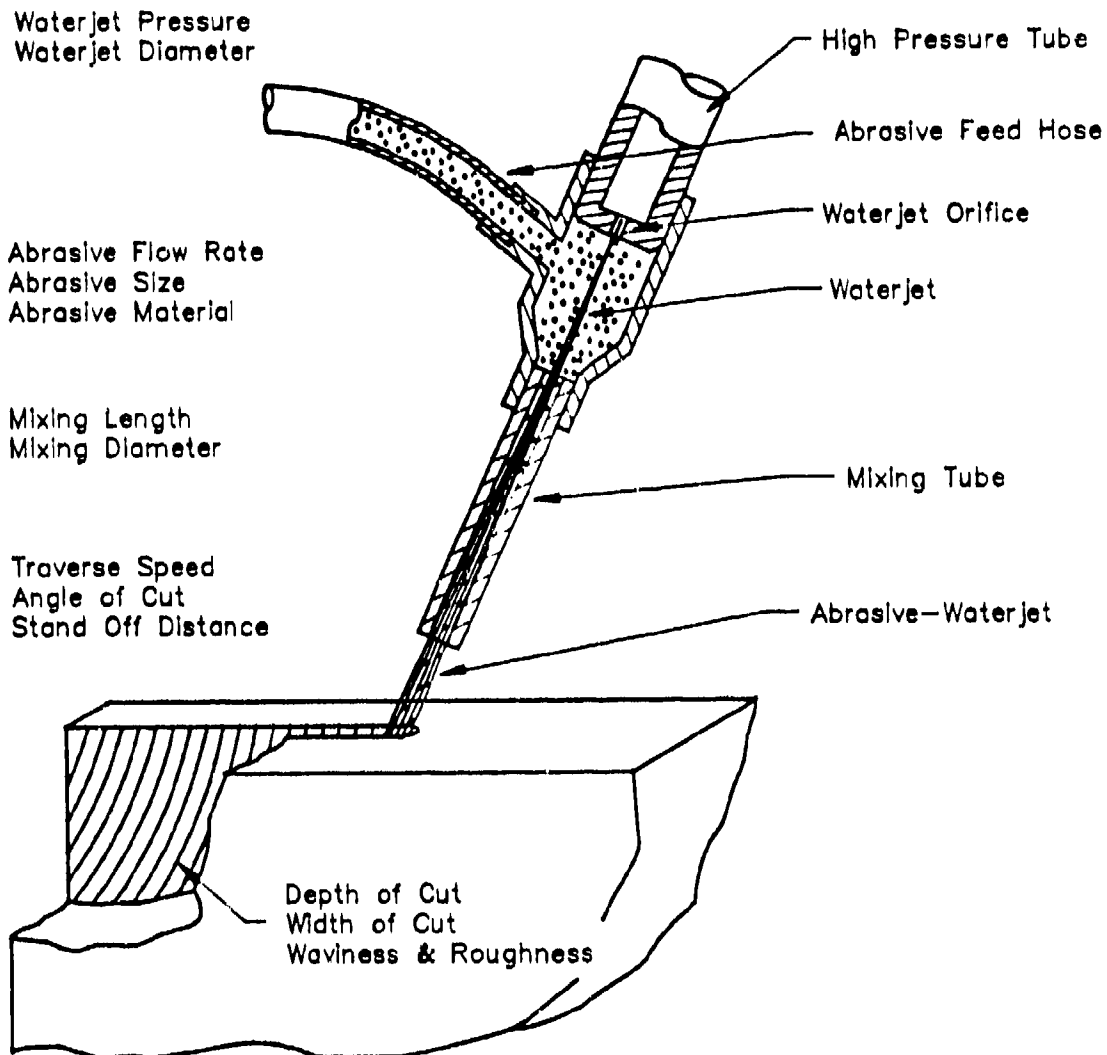
Figure 2. AWJ Nozzle Concept and Parameters
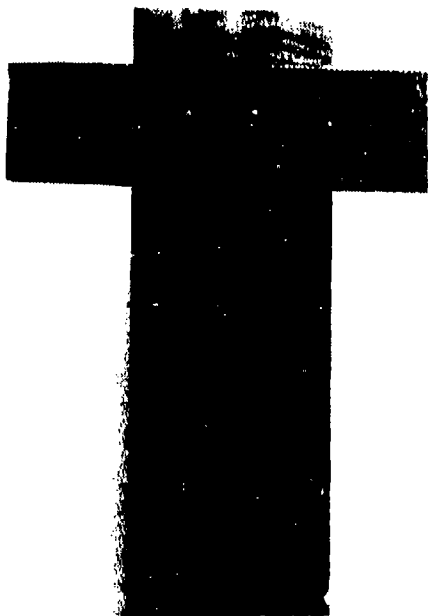
a-Cutting of laminated armor glass

b-Milling in brittle materials
(glass)

c-Turning of metal matrix composites
(Magnesium boron carbide)

d-Piercing in brittle materials
(Float glass)

Figure 3.   Examples of Machining with AWJ

shape and another to finish the part. Tensile tests conducted on turned parts indicated that AWJ machining does not alter the tensile characteristics of the material.

2.3 Single-Angled Rotary AWJ

The concept of a single-angled jet in a circular tube was selected for this study because of its versatility, ease of manufacture, and ease of application. The single-angled rotary AWJ tool consists of a stem, a high-pressure tube, a nozzle, and water and abrasives swivels, as shown in Figure 4. Abrasives flow to the nozzle through the annulus between the high-pressure conduit and the outer stem. The waterjet nozzle is machined so that the jet exits at nominally the same angle as the inclination of the mixing tube. The life expectancy for a mixing tube depends on a number of factors, such as the waterjet pressure, the tube diameter, and the abrasive flow rate. The outer stem of the tool used in this study was 0.75 inch in diameter.

H.P. WATER

ABRASIVES

ABRASIVE SWIVEL

HOUSING

ABRASIVE TRANSPORT TUBE

ULTRAHIGH-PRESSURE WATER

ULTRAHIGH-PRESSURE ORIFICE

MIXING THROAT
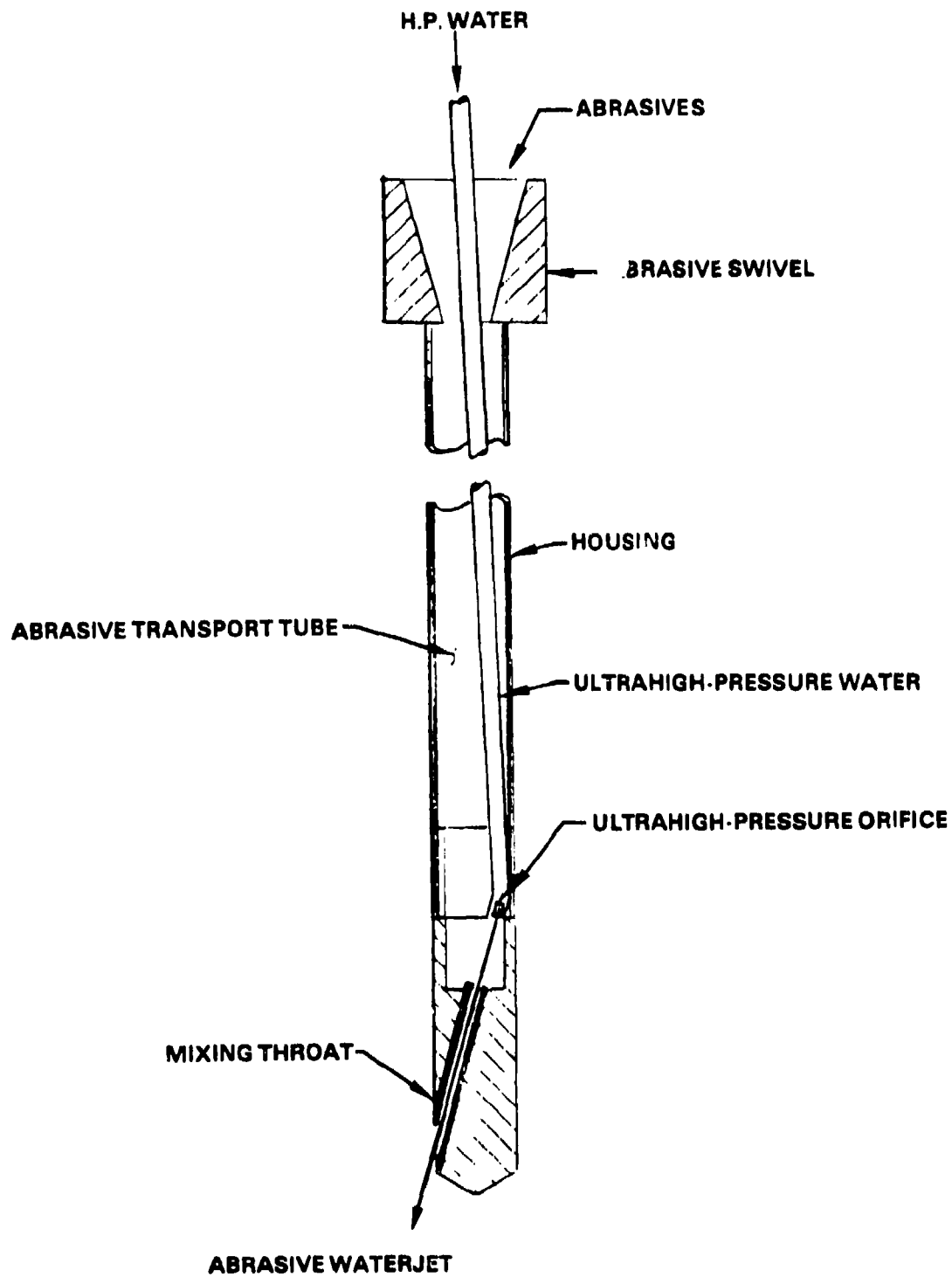
ABRASIVE WATERJET

Figure 4.   Single-Angled Rotary AWJ Tool

3. OBJECTIVES

The main objective of this Phase I research program was to determine the overall feasibility of using abrasive-waterjets to machine isogrid structures to net shapes. The specific objectives were to:

(1) Determine the AWJ parameters for linear cutting of isogrid patterns;

(2) Determine the AWJ parameters for milling of isogrid patterns;

(3) Investigate the feasibility of isogrid manufacturing using AWJ cutting and diffusion bonding; and

(4) Estimate the economics of AWJ machining of isogrid structures.

The results of these tests are presented in Section 5.

4. TECHNICAL APPROACH

The technical approach in this research was basically experimental and was supported by economic analyses. The work focused on using AWJs for the net-shape machining of isogrid patterns on the internal wall of aluminum tubes. Mockup parts were machined to include the basic geometries of actual isogrid patterns.

To achieve the objectives of this study, the work was divided into the following tasks:

Task 1 - Experimental Preparation

Task 2 - Exploratory Milling Tests with AWJs

Task 3 - Milling of Mockup Isogrid Patterns

Task 4 - Economic Analysis

The exploratory milling tests (Task 2) were conducted to evaluate the feasibility of three different approaches:

(1) Linear cutting then diffusion bonding an external skin on the tube

(2) Milling with a single-angled rotary AWJ

(3) AWJ milling with a steel mask

The results of these tests are presented in Section 5. An investigation was also made of the feasibility of using diffusion bonding, as proposed in the first approach. The results of this investigation are discussed in Section 6.

The demonstration milling tests (Task 3) were conducted using the most feasible approach, as determined in Task 2, to study the process in detail. The results of the demonstration tests are presented in Section 7.

The economic analysis (Task 4) was conducted to estimate the approximate cost of machining isogrid structures using AWJs. The analysis is presented in Section 8.

5. EXPERIMENTAL INVESTIGATION

The experimental results obtained with the three different approaches to isogrid machining are described in this section. For each approach, we first describe the experimental setup, then we discuss the quantitative and qualitative results obtained with that approach.

5.1 Linear Cutting of Isogrid Patterns

A conventional abrasive-waterjet nozzle was mounted on a linear traverse mechanism to cut aluminum and steel plates. These tests were conducted to evaluate the first machining approach and to obtain data on steel and aluminum cutting applicable in evaluating the third approach. The first approach involves two steps: (1) through-cutting of an isogrid pattern in aluminum tubes where cutting can be performed from either the inside or outside of the tube, and (2) bonding of an aluminum skin on the outside wall of the machined aluminum tube. Although aluminum cutting rates can be predicted using the equation given below, tests were conducted for confirmation. Aluminum cutting rates can be used to determine the total isogrid machining time and cost.

The linear cutting data are also important for evaluating the third machining approach, in which a mask or template made from an erosion-resistant material, such as steel, is used. The isogrid pattern is cut in the mask, which is then mounted inside the aluminum tube to be milled with the isogrid pattern. Cutting tests were conducted to compare the erosion rate of the steel relative to aluminum; and it was confirmed that steel masks could be used repeatedly. High-strength steels and carbides will offer more durable masks. The use of mild steel, however, which is relatively inexpensive, is adequate for concept demonstration.

Pattern cutting in aluminum and steel with AWJs can be achieved to produce accurate parts free from distortions or residual stresses. The cutting rates can be predicted from the following equation (Hashish, 1989b):

$$\frac{h}{d_j} = 0.282 \, c \, \frac{N_4}{N_2 N_3} + \frac{(1 - N_1)^2}{\dfrac{N_2 N_3}{1-c} + C_f \, (1-N_1)}$$

where h is the depth of cut, d_j is the AWJ diameter, c is an experimental factor, C_f is the frictional drag coefficient, and N_1, N_2, N_3 and N_4 are as follows:

$$N_1 = \frac{V_c}{V} \qquad\qquad N_2 = \frac{\pi \, \epsilon \, d_j^2}{2 \, m_a \, V}$$

$$N_3 = \frac{u}{V} \qquad\qquad N_4 = \frac{\epsilon}{\sigma}$$

where V is the particle velocity, V_c is the critical particle velocity, ϵ is the material specific energy, m_a is the abrasive flow rate, u is the traverse rate, and σ is the flow stress.

Typical data for AWJ cutting of aluminum and steel are shown in Figures 5 and 6, respectively, while Figure 7 shows agreement between predictions using the above equation and experimental results.

Because the cutting rate equation cannot predict the quality of cuts, a number of tests were conducted to cut 0.25-inch-thick aluminum and steel at different rates, slower than the maximum cutting speed, to obtain relatively smooth, straight cuts. The cutting conditions were:

$$\text{Waterjet pressure, } p = 50 \text{ ksi}$$
$$\text{Waterjet orifice size, } d_n = 0.018 \text{ inch}$$
$$\text{Mixing tube diameter, } d_m = 0.047 \text{ inch}$$
$$\text{Mixing tube length, } l_m = 4 \text{ inches}$$
$$\text{Abrasive flow rate, } m_a = 1.52 \text{ lb/min}$$

The observed cutting speeds to obtain relatively smooth cutting edges reached 30 and 10 in./min for aluminum and steel, respectively. Figure 8 shows the kerf width data obtained at the different cutting speeds. The variation in kerf width implies that the edges of the isogrid webs may be tapered. From a structural point of view, this may be superior to straight-walled webs. It should be mentioned here that straight walls can be obtained using the AWJ by varying the jet parameters.

The total cutting time for isogrid patterns will be discussed later for both aluminum and steel masks.

5.2 Milling with Single-Angled Rotary AWJ

A limited experimental effort was conducted using a single-angled rotary AWJ tool for the milling of isogrid patterns. Figure 9 shows the experimental setup for milling with the rotary AWJ tool. The aluminum sample is mounted on a work table inside the catcher tank. The rotary AWJ tool is mounted on a traverse mechanism above the catcher and work table.

A total of six milling tests were conducted to study the degree to which the milling depth can be controlled. Due to the rotary motion of the advancing tool, material exposure to the jet is not uniform, i.e., the circular passes of the jet are concentrated near the edges of the cut along the direction of cross feed. This lack of uniformity leaves a "W"-shaped slot that is deeper near the edges than over the central area, which is relatively uniform in depth. This "W"-shaped cavity can be made more uniform by masking the edges so that, in these areas of concentrated jet overlap, the jet is impinging on the mask rather than in the target material. Figure 10 shows milled aluminum samples using the rotary tool with masked edges at different degrees of overlap. The overlap is controlled by the cross-feed rate and rotational speed as given in the appendix. Note that test number 64 produced noticeable "tool marks," while other
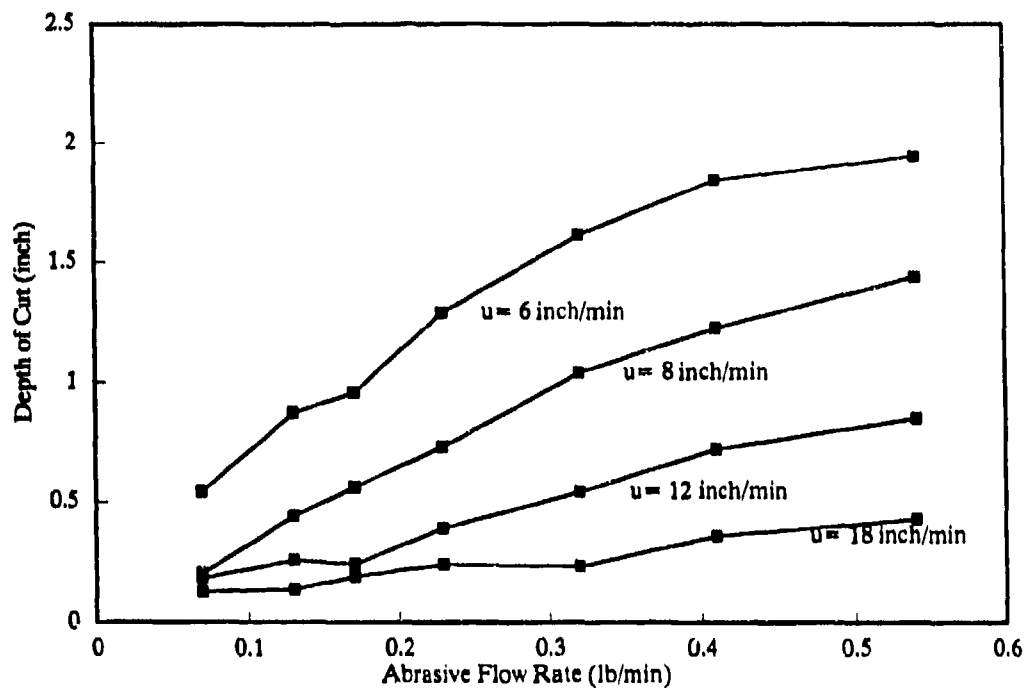
Figure 5.   Effect of Abrasive Flow Rate on Aluminum Cutting
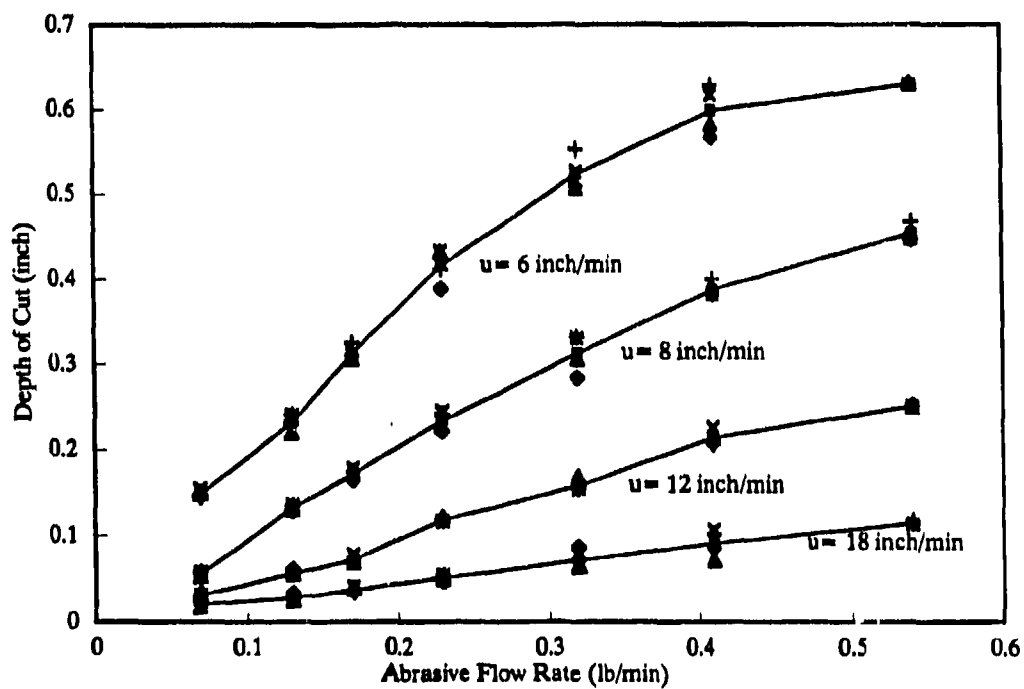
Figure 6.   Effect of Abrasive Flow Rate on Steel Cutting
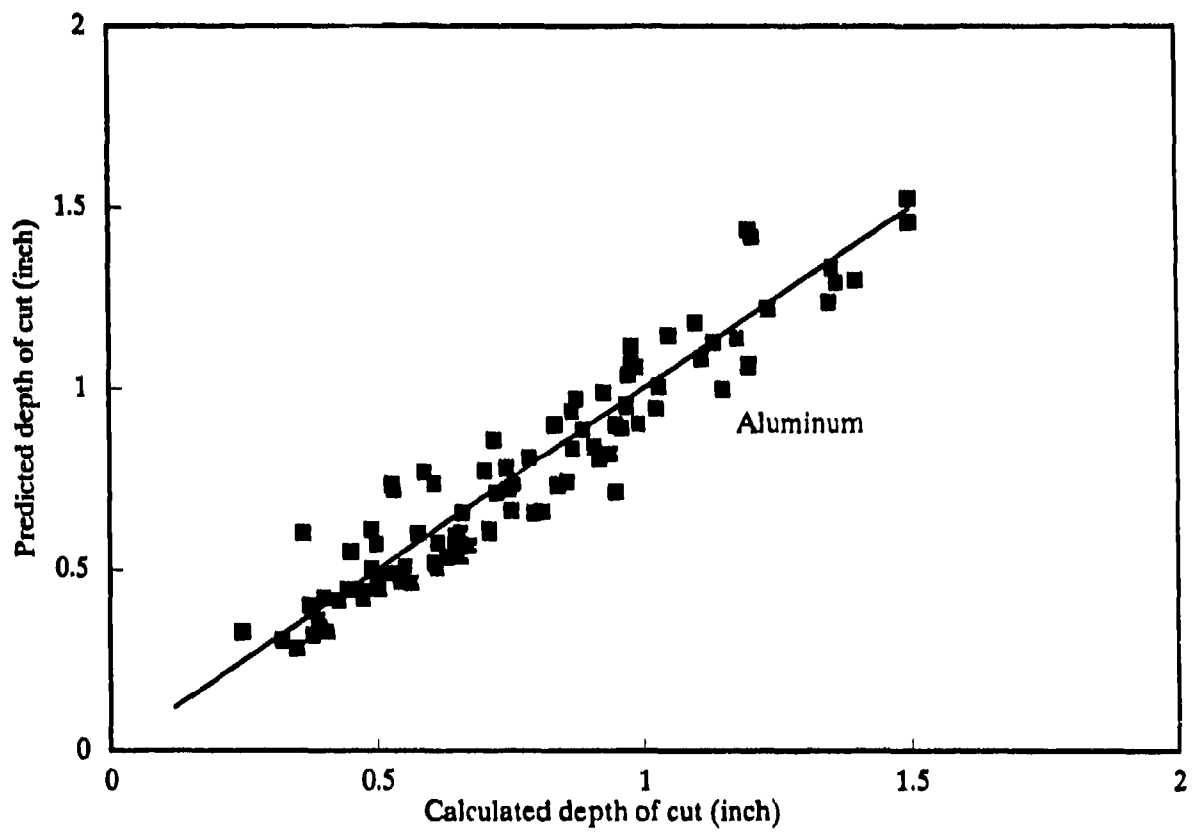
Figure 7. Prediction of Depth of Cut in Aluminum
Versus Experimental Observation
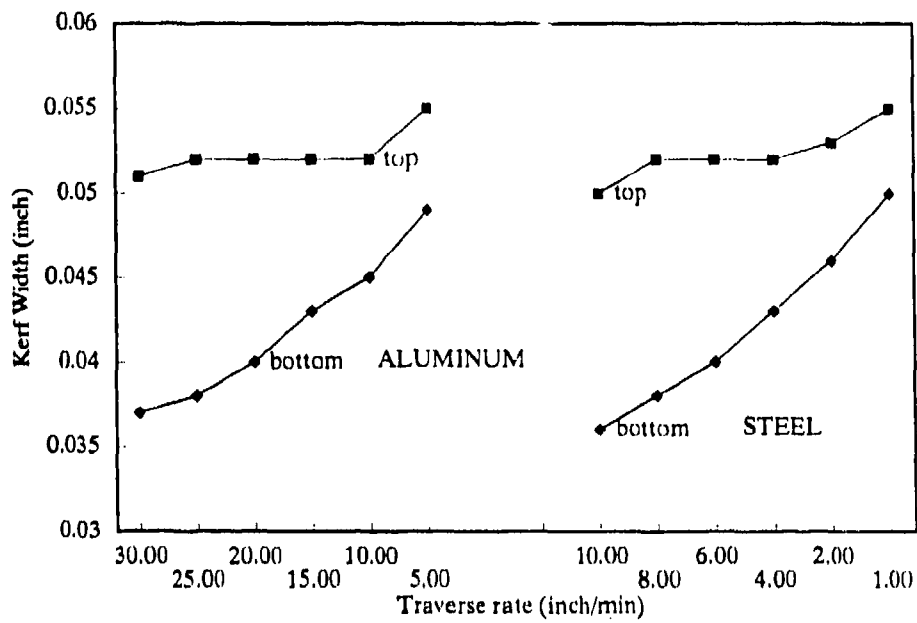
Figure 8.   Linear Cutting of Steel and Aluminum
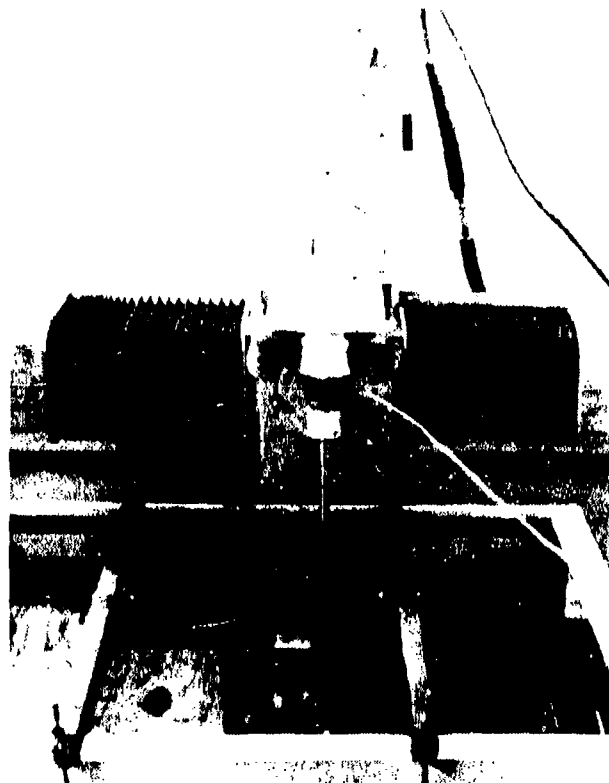
Figure 9.   Experimental Setup for Milling with Single-Angled Rotary AWJ Tool
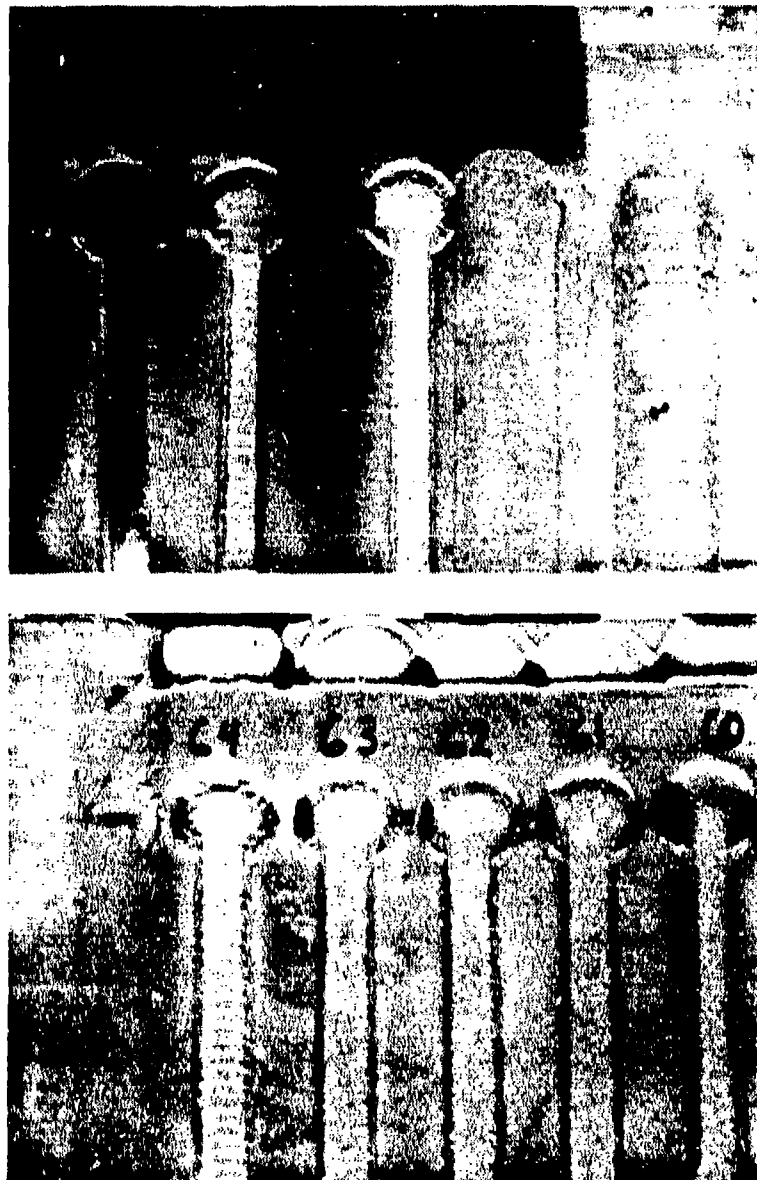
Figure 10.   Single-Angled Rotary AWJ Tool Milling Results

cuts do not show such marks and have similar surface topography. Visual inspection of the pocket depth indicates that the mask has significantly reduced the depth variation.

5.3   Milling with Conventional AWJ Nozzle

This milling approach proved to be the most feasible and consequently represented the majority of the experimental investigation. In this section, we describe the milling test setup, experimental procedure, and results.

5.3.1   Milling Test Setup

An experimental test setup was prepared to conduct the milling experiments on curved mockup cylindrical parts that would simulate actual parts. A typical isogrid pattern was included in these experiments.

An overview of the isogrid milling system used for the isogrid pattern generation tests is shown in Figure 11. The system contained two axes of motion, cross-feed (linear traverse) of the AWJ tool and part rotation. The rotating motion was used to produce the high rate of linear speed between the nozzle and the sample (4,000 to 12,000 in./min); this high rate is difficult to achieve using a linear traverse system. The cross-feed motion of the AWJ tool was used to control the amount of overlap of the AWJ from one revolution of the drum to the next. Both motions were driven by DC servo motors and were computer controlled. Cross-feed and rotary motion parameters could be varied by changing the computer program, which facilitated rapid testing.

Figure 12 shows the milling setup in more detail. The samples were placed in the drum and covered with a mask in which the desired isogrid pattern had been AWJ cut. Figure 13 shows a typical mask. The masks were made of mild steel for ease of manufacture and low cost; however, for production of parts, the masks could be made of harder material such as tungsten carbide which would increase their useful life time. This test setup provided the ability to change several parameters. Waterjet orifice size could be changed by placing different orifices in the abrasive jet assembly. The mixing tube length and diameter can be varied by replacing the mixing tubes in the abrasive jet assembly. The abrasive jet mounting bracket is adjustable in the vertical direction to allow variation in the standoff distance.

Figure 14 shows an assembly drawing of the rotating drum mechanism designed and built specifically for these tests. The drum is mounted on a shaft supported by two bearings. A three-to-one reduction chain drive connects the drum shaft to the drive shaft. The drive shaft is connected to a DC servo motor through a flexible coupling.
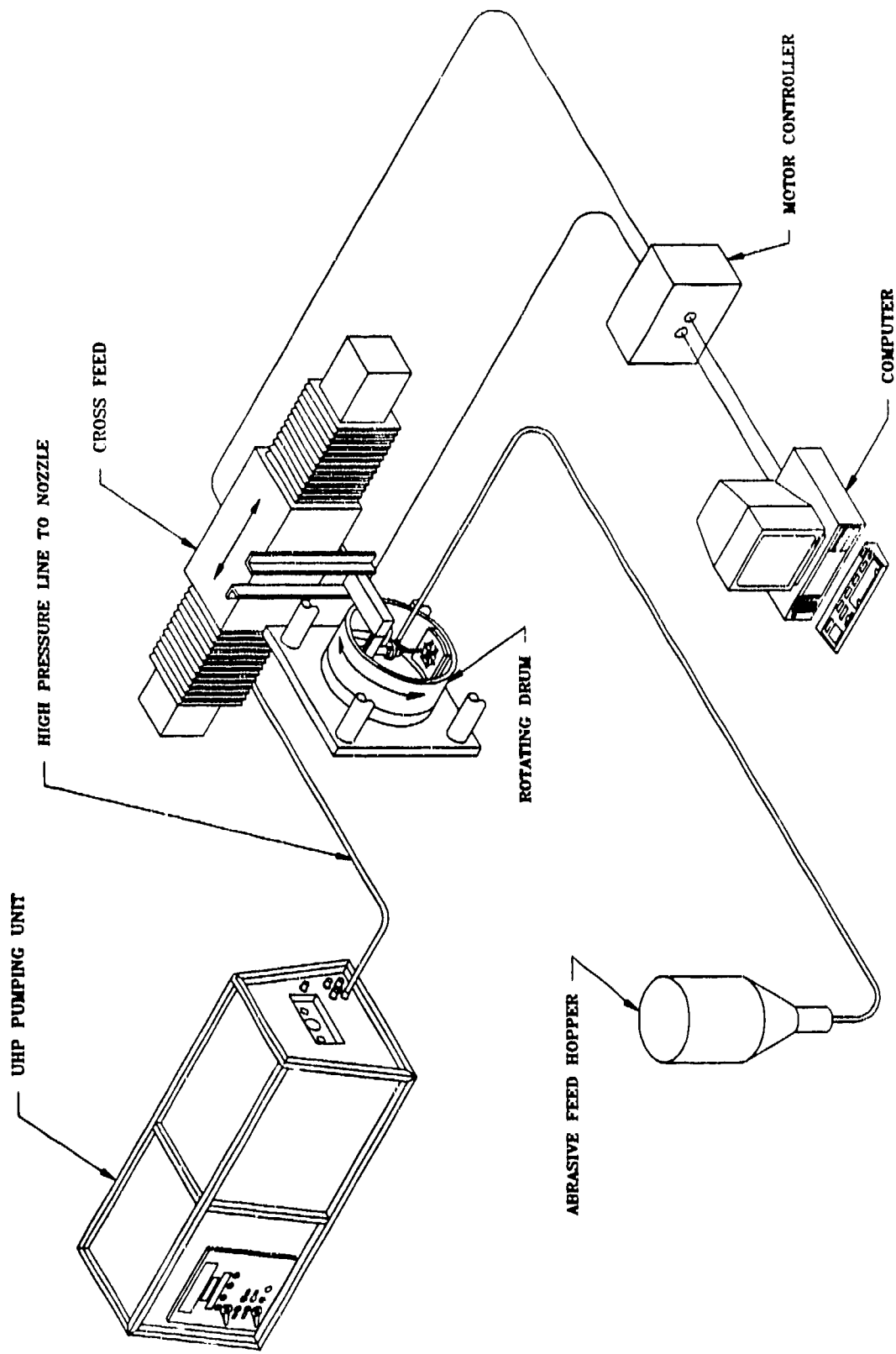
Figure 11. Milling Setup Showing System Components

MOTOR CONTROLLER

CROSS FEED

HIGH PRESSURE LINE TO NOZZLE

ROTATING DRUM

COMPUTER

UHP PUMPING UNIT

ABRASIVE FEED HOPPER

CROSS FEED

UHP WATER LINE

ABRASIVE FEED LINE

MASK

TEST SAMPLE

ABJET NOZZLE

ROTATING DRUM

STATIONARY FRAME
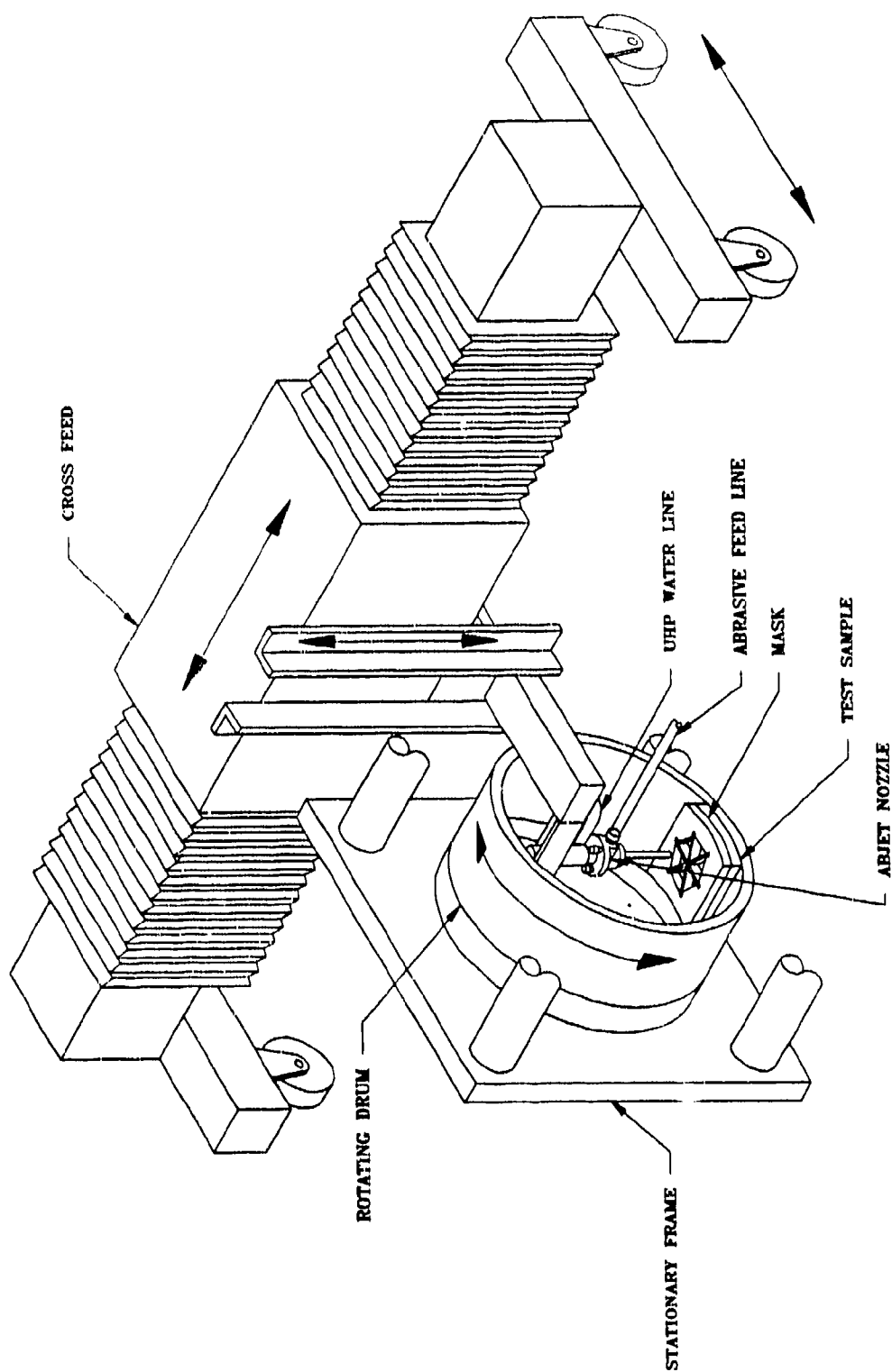
Figure 12. Milling Setup Showing Traverse Components
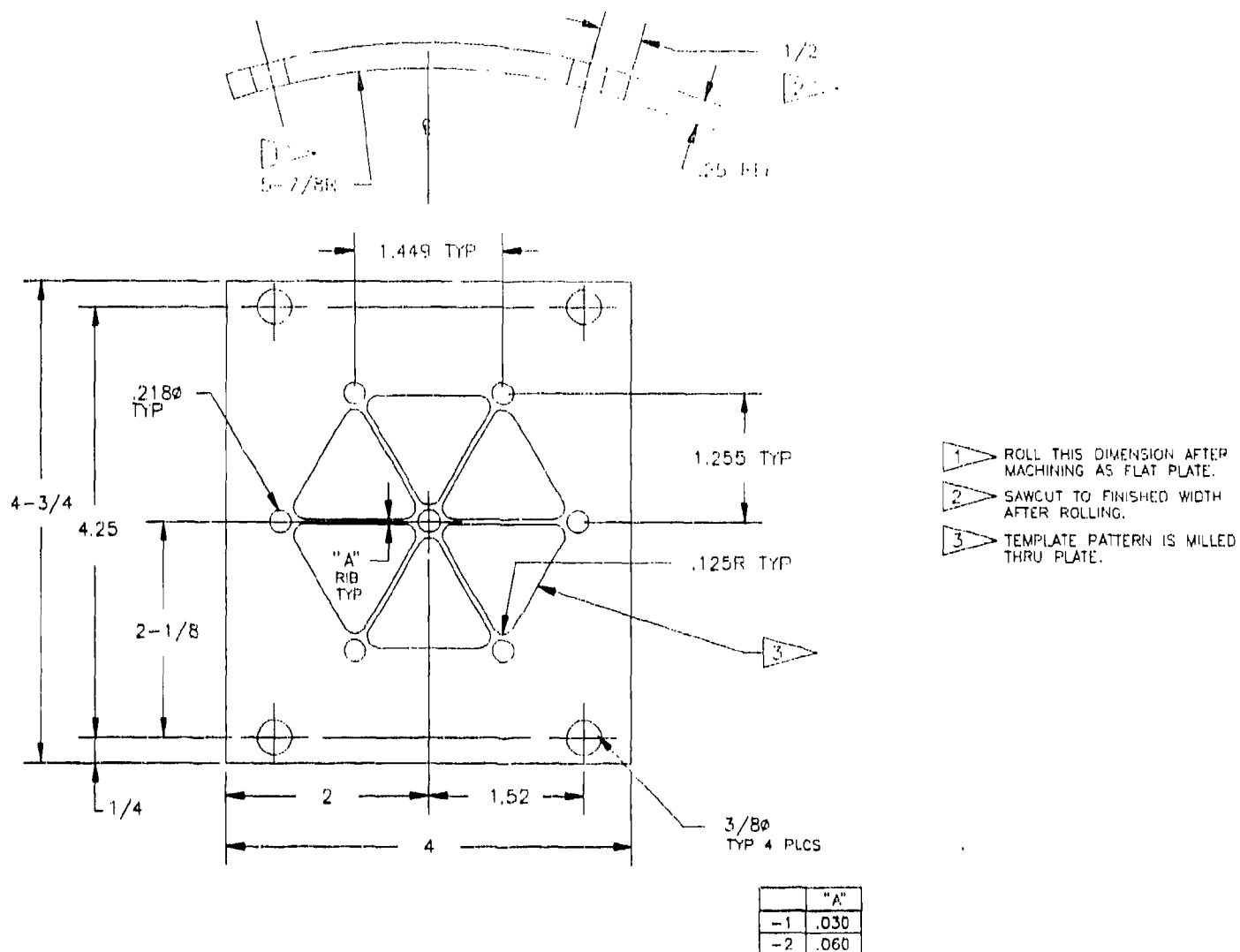
Figure 13. Mask Geometry
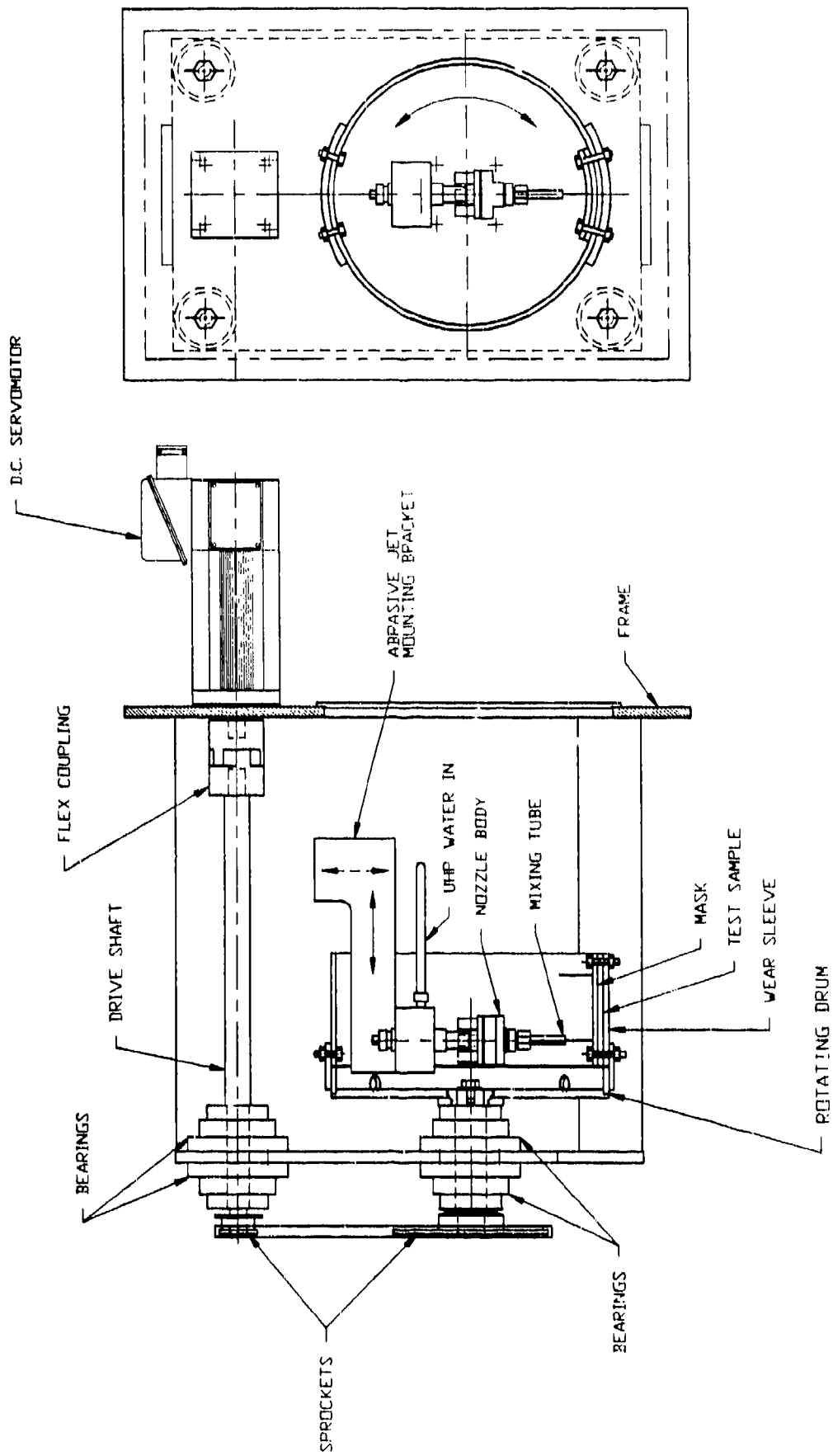
Figure 14. Details of Milling Arrangement

Labels in figure: D.C. SERVOMOTOR, ABRASIVE JET MOUNTING BRACKET, FRAME, FLEX COUPLING, UHP WATER IN, NOZZLE BODY, MIXING TUBE, MASK, TEST SAMPLE, WEAR SLEEVE, DRIVE SHAFT, ROTATING DRUM, BEARINGS, BEARINGS, SPROCKETS

5.3.2 Experimental Plan

The experimental plan devised for milling tests focused on jet-material interaction parameters. These parameters are:

- Degree of overlap (or cross-feed rate)
- Standoff distance (of AWJ nozzle)
- Traverse rate
- Particle size

- Pressure
- Abrasive flow rate
- Waterjet diameter
- Milling to thin wall
- Rotation speed

Figure 15 shows the strategy of tests for milling. The base point parameters that were selected represent effective AWJ cutting parameters for aluminum. Variations around the base point were aimed at defining directions of improved parameters. The plan was dynamic in nature, i.e., it was modified based on the milling observations as they were generated. The experimental investigation started with exploratory tests which were conducted to actually help in setting up the experimental plan. The appendix lists the parameters and results of the milling tests. Rather than conducting a factorial test matrix, a simplified approach was used. In this approach, tests were conducted in sets of five. The best set of parameters was used in the next series of tests.

The starting parameters for milling were:

Waterjet pressure: 45 ksi
Waterjet orifice size: 0.013 inch
Abrasive flow rate: 0.52 lb/min
Abrasive material: garnet
Particle size: 120 mesh
Mixing tube length: 3 inches
Mixing tube diameter: 0.047 inch
Traverse rate: 4,000 in./min

The test procedure was as follows:

(1) Prepare a computer spreadsheet to list the tests to be conducted and record the data.
(2) Prepare a mask with holes drilled as shown in Figure 16.
(3) Take a sample of aluminum and weigh it.
(4) Mount the aluminum sample under the mask.
(5) Conduct milling test at the selected condition.
(6) Remove sample and weigh it.
(7) Enter weight of sample and milling area into the computer spreadsheet.

Degree of Overlap

Base Point

P=45 ksi
d_n =0.013 inch
d_m =0.040 inch
u=4000 in/min
m_a =0.53 lb/min
garnet mesh 100

Value 1

Value 2

Value 3

Value 1

Value 2

Value 3

Stand
Off
Distance

Variable "n"

Value 1

Value 2

Value 3

Branch to
Variable (n+1)
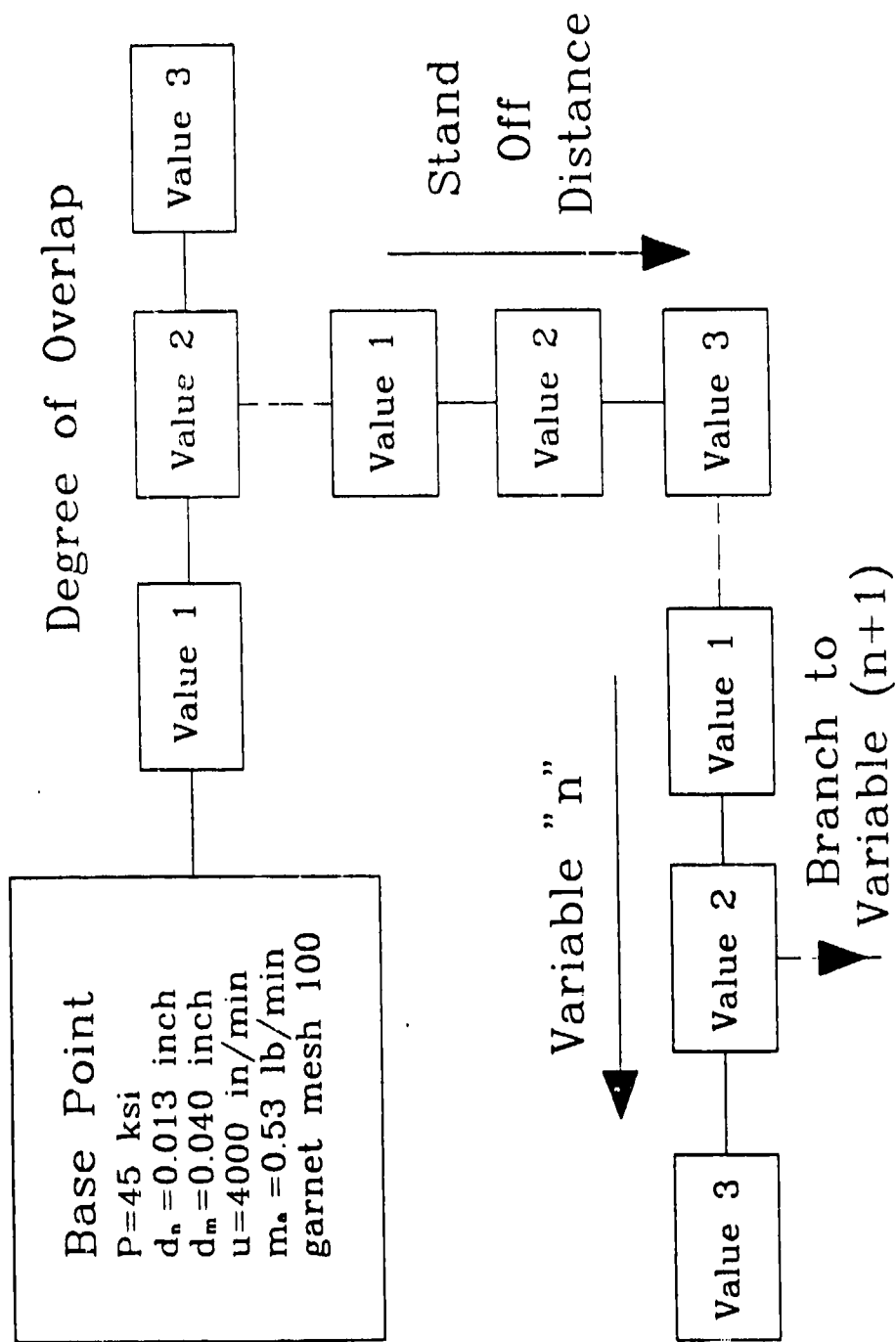
Figure 15.   Experimental Plan Tree
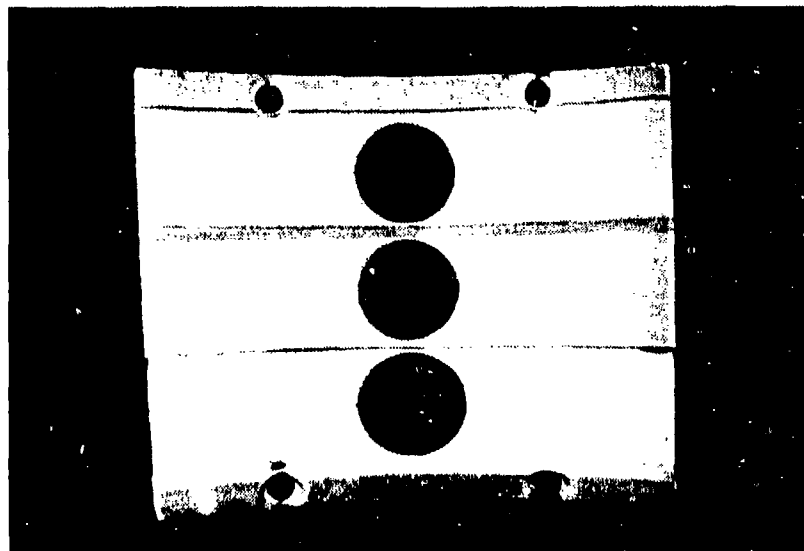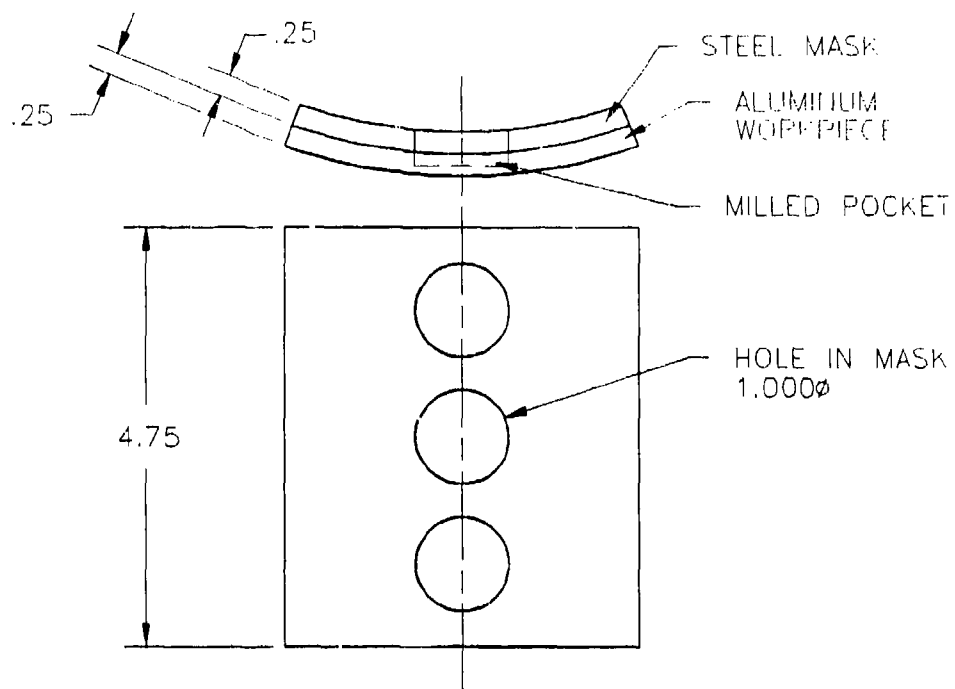
Figure 16. Simplified Mask for Milling Tests

The objectives of the milling tests were to:

- Determine volume removal rates.
- Determine the accuracy of milling to a specified depth.
- **Determine milling data trends.**

In the following section, we present detailed observations made from the experimental results.

5.3.3 Experimental Results

The degree of overlap is expressed as the ratio of the cross-feed increment per revolution of the part to the mixing tube diameter, as illustrated in Figure 17. Figure 18 shows the effect of the degree of overlap on the volume removal rate for three different mixing tube diameters (see appendix, test numbers 4 to 18). The highest volume removal rate is obtained with the smallest mixing tube diameter. This result is attributed to the fact that more effective jets are obtained with smaller-diameter mixing tubes. The cross-feed rate was adjusted according to the mixing tube diameter and the required degree of overlap. For large mixing tubes, a higher cross-feed rate was used to maintain a similar overlap rate as compared to a smaller mixing tube.

The volume removal rate peaks at certain overlap ratios. Figure 19 shows the corresponding depth of milling per pass, indicating that maximum depth values do not correspond to conditions of highest volume removal rate (see appendix, test numbers 4 to 18). The effect of cross-feed rate is also represented in Figures 18 and 19 by the degree of overlap. From Figure 19, it is obvious that as the degree of overlap (and consequently the cross-feed rate) increases, the depth of milling per pass decreases. This depth per pass determines the accuracy or resolution of milling. Thus, to enhance the accuracy to 0.001 inch with $d_n/d_m = 0.013/0.047$, for example, an overlap of 0.8 or 1 must be used. Fortunately, an overlap of 0.8 still yields the maximum volume removal rate. For other milling conditions, however, optimization of the volume removal rate and milling accuracy will be an important task.

Figure 20 shows different milling patterns for the data given in Figures 18 and 19 Observe that the lay of the milled cavities is in the direction of the traverse. This is illustrated schematically in Figure 21 (see appendix, test numbers 4 to 18) and is expected to occur as in conventional milling. However, the depth of milling variation due to lay can also be controlled by the degree of overlap, as shown in Figure 20 (see appendix, test numbers 4 to 18). No efforts were made in this phase to quantify the details of surface morphology. Only magnified inspection was used to select conditions for subsequent testing.
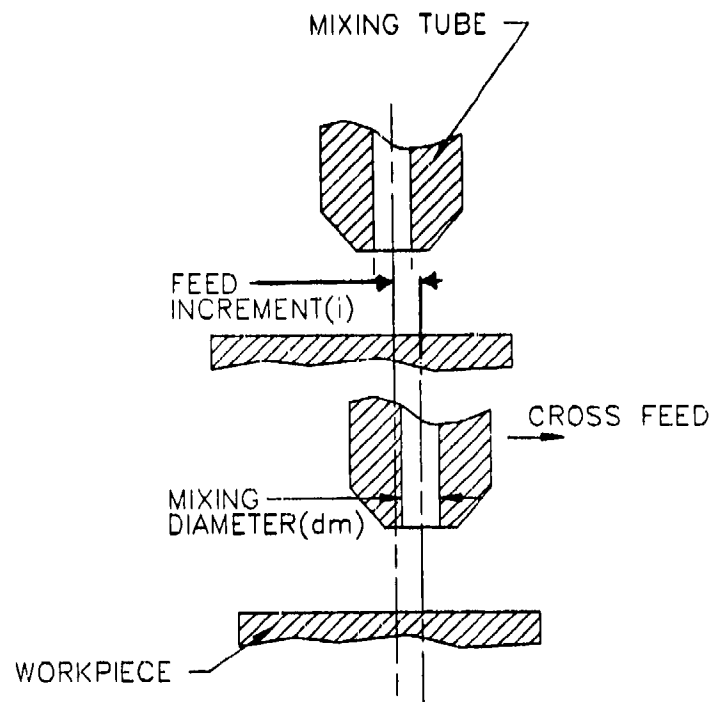
Figure 17.   Schematic of AWJ Overlap
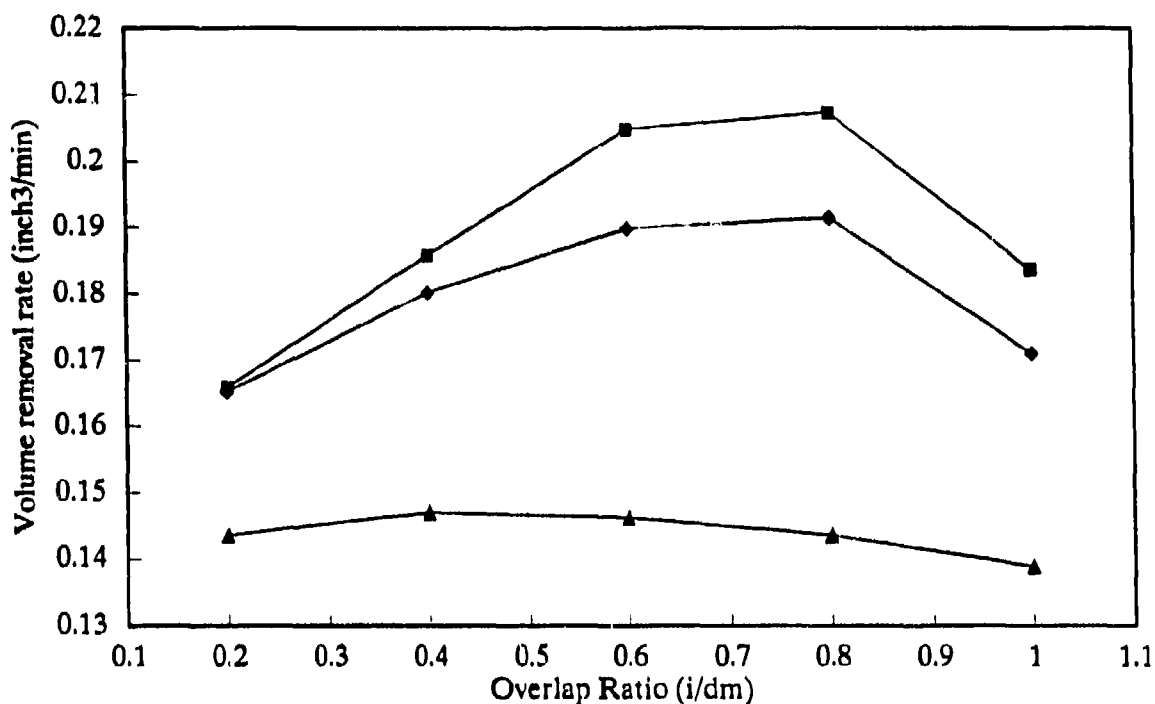
Figure 18. Effect of Overlap on Volume Removal Rate for Three WaterJet/Mixing Diameter Combinations. p = 45 ksi, l_m = 3 inches, m_a = 0.53 lb/min, gs mesh 100
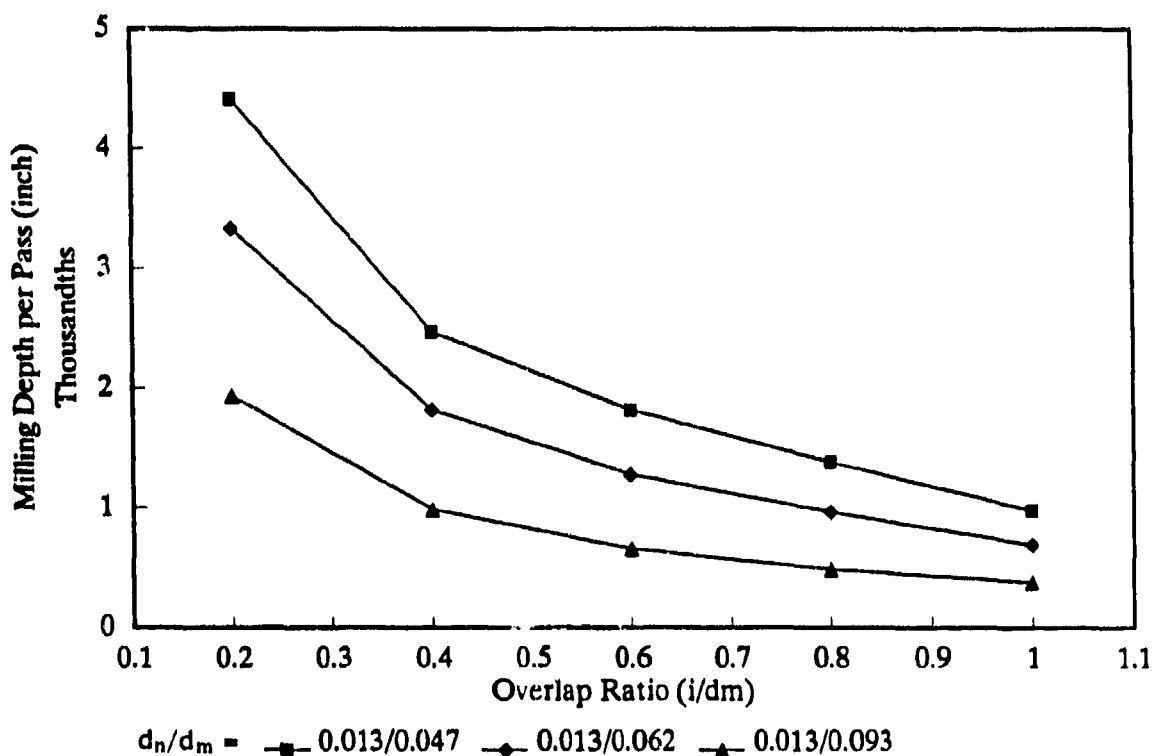
Figure 19. Milling Depth Versus Degree of Overlap for Three WaterJet/Mixing Diameter Combinations. p = 45 ksi, l_m = 3 inches, m_a = 0.53 lb/min, gs mesh 100

Figure 20. Milling Patterns for Different Degrees of Overlap for Data Presented in Figures 18 and 19. $p = 45$ ksi, gs mesh 100, $d_n = 0.013$ inch, $m_a = 0.53$ lb/min (numbers under photos indicate corresponding test number in appendix)
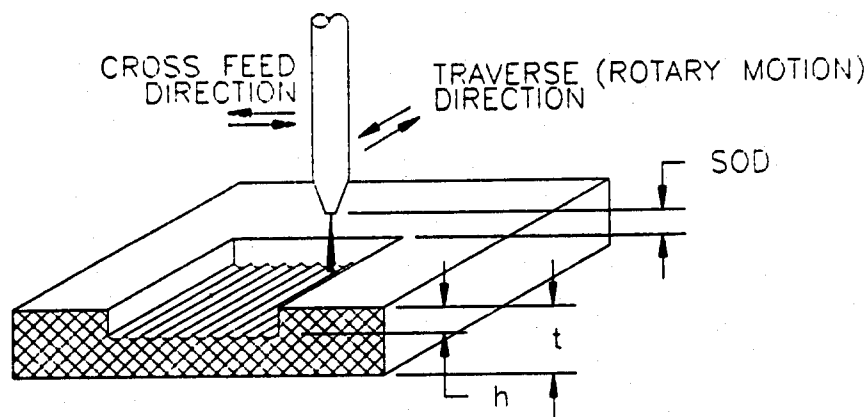
Figure 21. Pocket Milling Geometry and Surface Lay
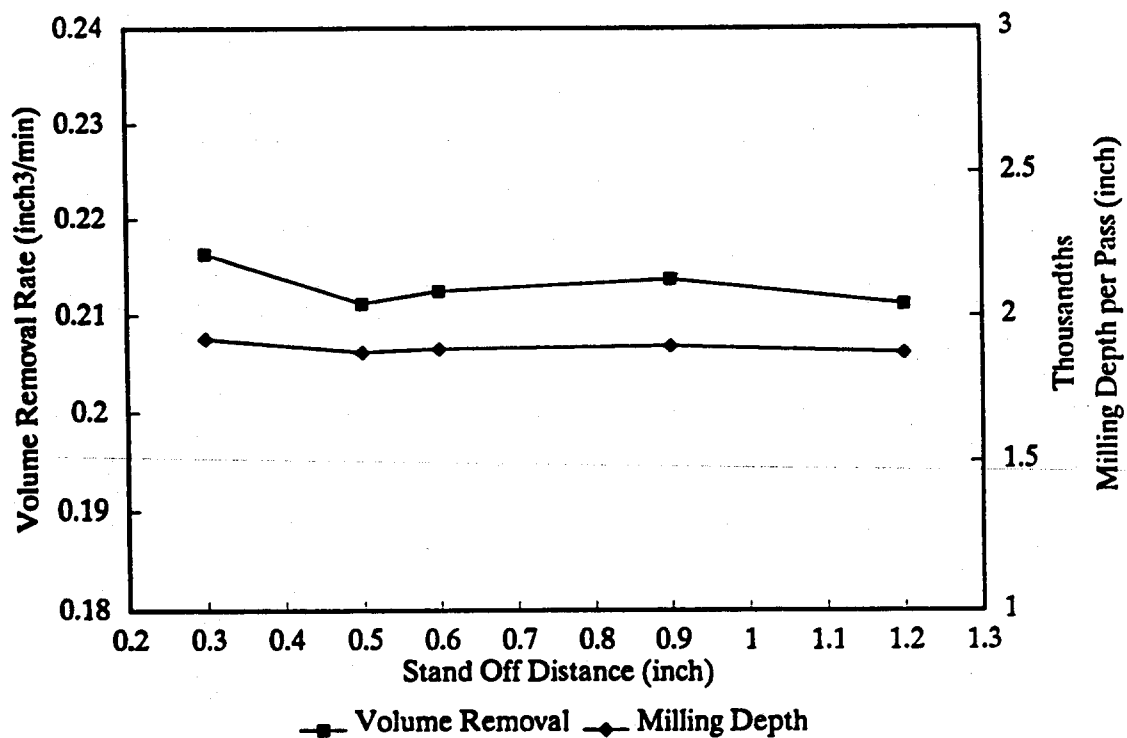
Figure 22. Effect of Standoff Distance on Volume Removal Rate and Milling Depth Per Pass. $p = 45$ ksi, gs mesh 100, $d_n = 0.013$ inch, $d_m = 0.047$ inch, $l_m = 3$ inches, $m_a = 0.53$ lb/min, inc $= 0.6$ (see appendix test numbers 19 to 23)

The effect of standoff distance at an overlap ratio of 0.6 is illustrated in Figure 22 (see appendix, test numbers 19-23). It is observed that varying the standoff distance between 0.3 and 1.2 inches did not significantly change the volume removal rate or depth of milling per pass. Increasing the standoff distance will increase the actual degree of overlap. This is because the jet spreads, and its actual diameter at the material surface increases (though its effective core may reduce). In the data shown in Figure 22, the nominal overlap based on the mixing tube diameter is used (see appendix, test numbers 19-23). It should be mentioned here that the effect of increasing the jet diameter by changing the standoff distance is different than that of increasing the mixing tube diameter. In the latter case, the mixing efficiency may be reduced.

The effect of traverse rate (rotary motion) is illustrated in Figure 23 (see appendix, test numbers 20, 24-27). The traverse rate should be distinguished from the cross-feed rate. The traverse rate is more significant in controlling the jet-material interaction process and consequently the volume removal, while the cross-feed rate controls the exposure period over a given point in the workpiece through the number of passes. Obviously, high speeds will result in reduced depth of cut and consequently better control over tolerance. Also, increasing the speed over a certain limit results in a reduction in the volume removal rate, as observed in Figure 23. In our experiments, the traverse rate was controlled by the rotary speed, a well-controlled factor. Observe that a milling depth of 0.0007 inch is obtained. This does not represent the best resolution value for milling tolerance. Finer tolerances will be controlled by the particle size and surface topography more than by volume removal.

The effect of particle size on volume removal rate is illustrated in Figure 24 (see appendix, test numbers 26, 28-30). The surface topography for these tests is also shown in the same figure. Notice that a finer surface is obtained with finer abrasives. For mesh 150, however, a reduction in volume removal rate is observed. Smooth surface topography may not necessarily be an important criterion for isogrid milling as long as the structural strength and integrity of the part are not affected.

The effect of pressure on the volume removal rate and depth of milling per pass is illustrated in Figure 25 (see appendix, test numbers 26, 31-33). A nearly linear relationship is observed. The data also indicate that a low threshold pressure is required. To control the depth of milling at the end of a milling operation, the pressure may be reduced. This will reduce the depth of milling and provide accurate control.

As in linear cutting, the abrasive flow rate effect tends to taper off as the abrasive flow rate is increased. This is illustrated in Figure 26 (see appendix, test numbers 36-42). It is more efficient to utilize low abrasive flow rates for higher volume removal rates; however, improved surface uniformity may be obtained at higher abrasive flow rates. Figure 27 shows photographs
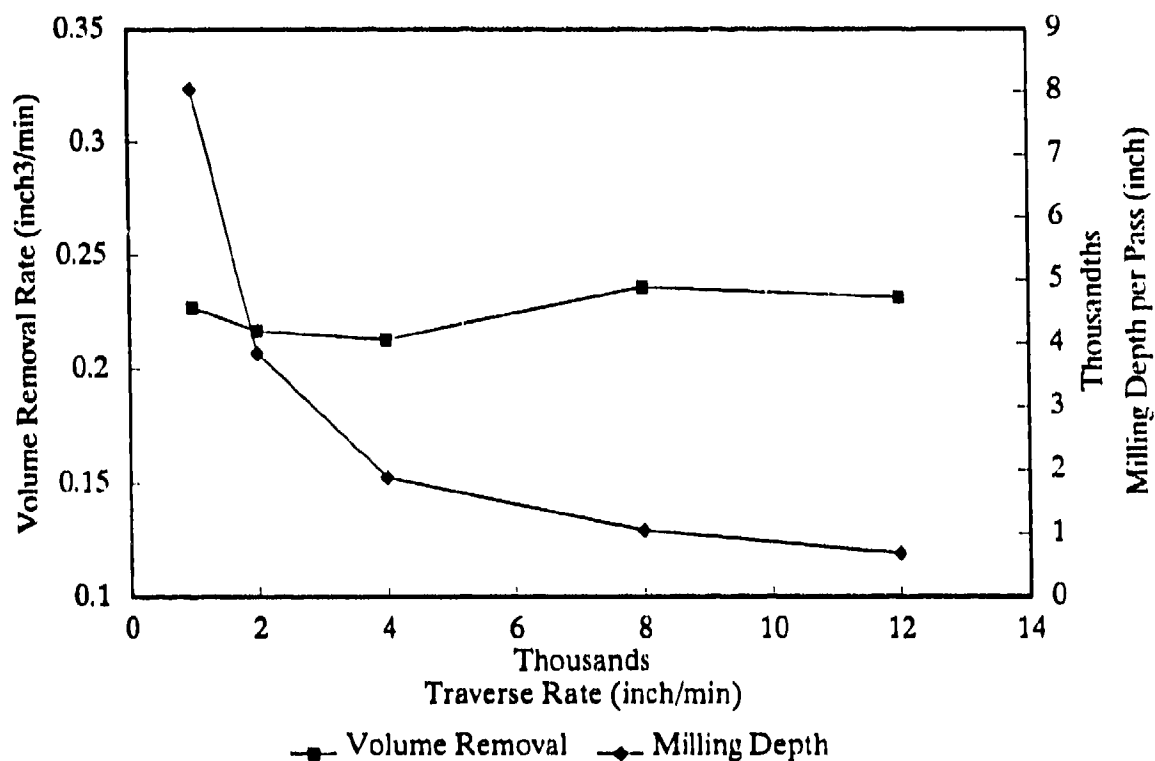
Figure 23. Effect of Traverse Rate (Produced by Rotating Drum) on Volume Removal Rate and Milling Depth Per Pass at Fixed Overlap Ratio of 0.6. p = 45 ksi, gs mesh 100, d_n = 0.013 inch, d_m = 0.047 inch, m_a = 0.53 lb/min, inc = 0.6 (see appendix test numbers 20, 24-27)
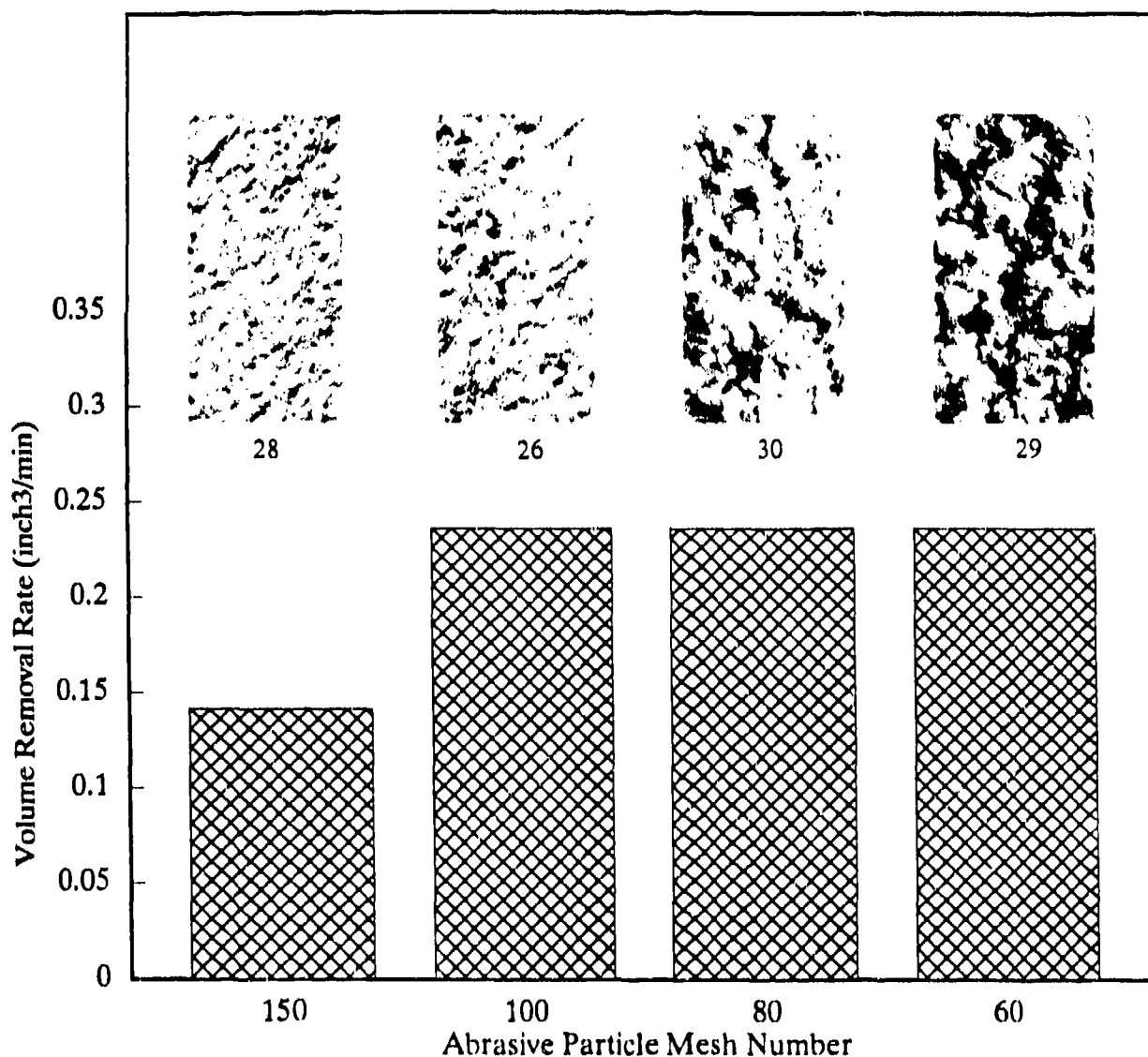
Figure 24. Effect of Particle Size on Volume Removal Rate and Surface Topography. p = 45 ksi, gs mesh 100, d_n = 0.013 inch, d_m = 0.047 inch, m_a = 0.53 lb/min, inc = 0.6, u = 6.18 in/min, n = 10.96 rps (numbers under photos indicate corresponding test number in appendix)
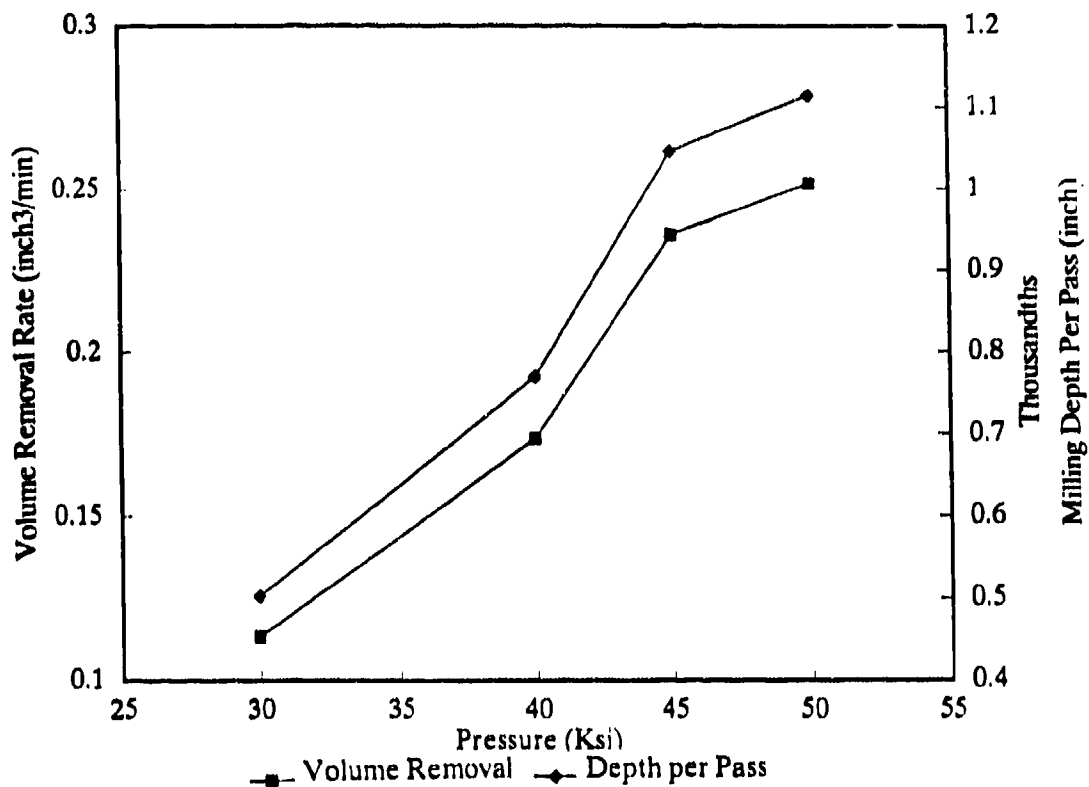
Figure 25. Effect of Pressure on Volume Removal Rate and Milling Depth Per Pass. d_m = 0.047 inch, l_m = 3 inches, d_n = 0.013 inch, gs mesh 100, m_a = 0.53 lb/min, n = 10.96 rps, inc = 0.6, u = 6.18 in/min (see appendix test numbers 26, 31-33)
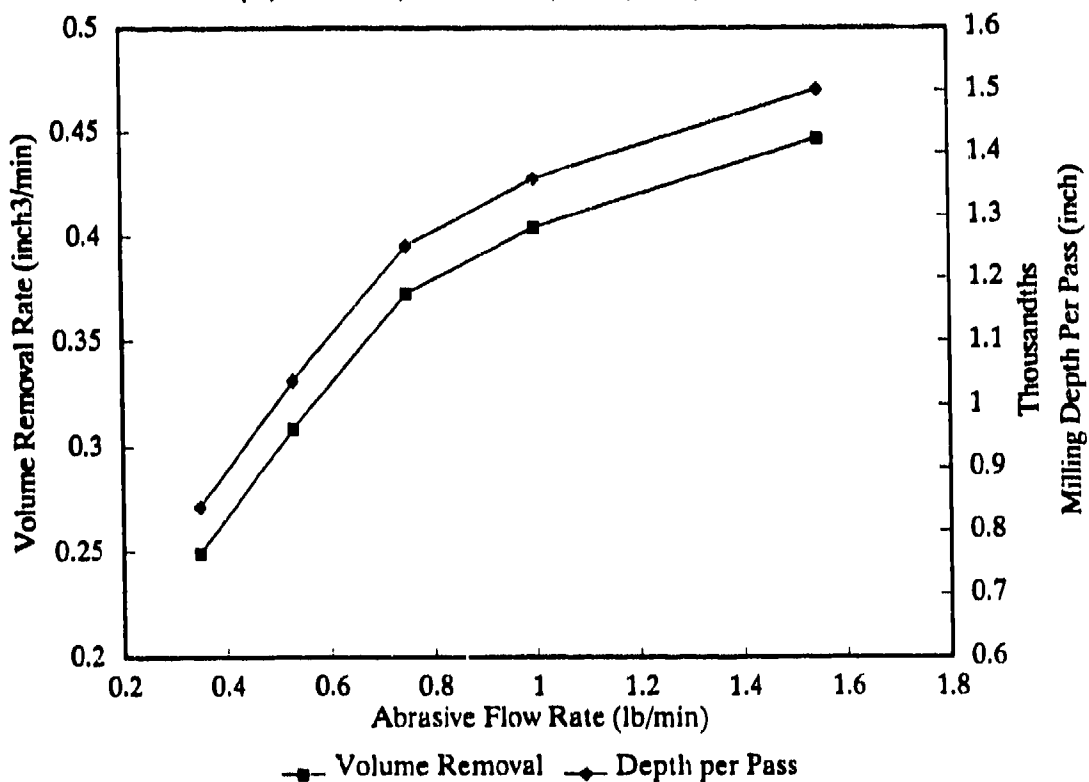
Figure 26. Effect of Abrasive Flow Rate on Volume Removal Rate and Milling Depth Per Pass. d_m = 0.047 inch, l_m = 3 inches, d_n = 0.013 inch, p = 45 ksi, gs mesh 100, n = 10.96 rps, inc = 0.6, u = 6.18 in/min (see appendix test numbers 36-42)

36

$m_a = 0.35$ lb/min

37

$m_a = 0.53$ lb/min

38

$m_a = 0.75$ lb/min

39

$m_a = 1.00$ lb/min

42

41
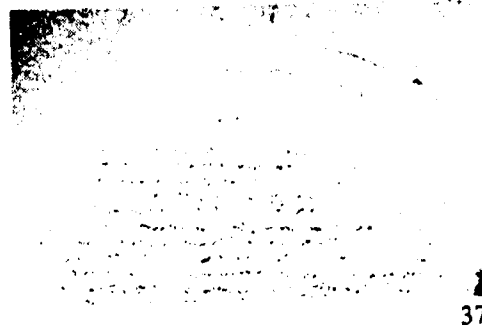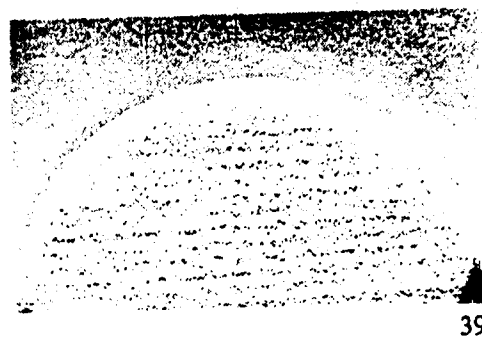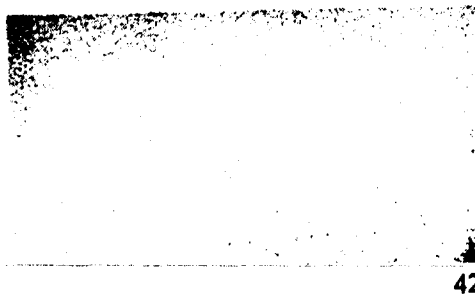
$m_a = 1.30$ lb/min
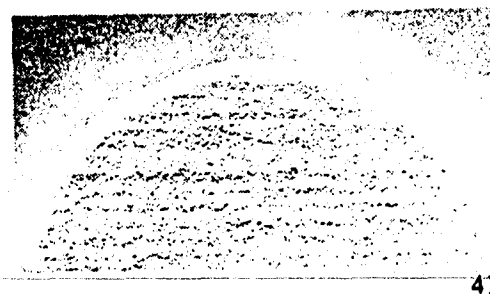
$m_a = 1.55$ lb/min

Figure 27.   Milling Patterns for Different Abrasive Flow Rates. $d_m = 0.047$ inch, $l_m = 3$ inches, $d_n = 0.013$ inch, $p = 45$ ksi, gs mesh 100, $n = 10.96$ rps, inc = 0.6, $u = 6.18$ in/min (see appendix test numbers 36-42)

of milled areas in which the above-mentioned advantage is not evident due to the relatively narrow range of abrasive flow rates used.

Figure 28 (see appendix, test numbers 31, 34-35) shows the effect of waterjet diameter on volume removal rate and depth of milling. It is observed that increasing the jet diameter from 0.009 to 0.018 inch will increase the volume removal rate from 0.16 to 0.43 in.^{3}/min, i.e., by less than 3 times, while the hydraulic power increased by a factor of 4. This indicates that small-diameter waterjets are more efficient. A milling system that uses multiple small-diameter waterjets will be more efficient than one that uses fewer jets at the same power level. This, of course, has practical limitations when considering the reliability and maintenance of the system.

Tests were also conducted to mill to required depths. Figure 29a (see appendix, test numbers 43-46) shows the progression of milling depth expressed as a function of the number of passes. Figure 29b shows the calculated average depth per pass. The data show that the milling rate is relatively linear with the number of passes, and a depth of 0.002 to 0.025 inch is obtained per pass. This represents the milling resolution at the selected condition.

The effect of mask thickness was observed in the course of the milling tests. Masks wear out and become thinner, but no significant effects were observed on the milled aluminum sections. Thin carbide masks (0.06 inch) were used in two tests (see appendix, test numbers 57-58). The carbide masks were simply disks with central holes. The milled aluminum patterns did not show any differences compared to those milled with 0.25-inch-thick steel masks. It was observed, however, that the perpendicularity of the mask's edges and its fit to the aluminum workpiece generally did have an effect on the milled edges. For example, if the mask is not in uniform contact with the workpiece, edges may not well represent the mask geometry, as shown in Figure 30. Observe the degree of out-of-roundness of the produced pocket hole.

No quantitative analysis was done to study the effect of mask wear on web thickness. It is expected, however, that excessive mask wear will affect the number of times a mask can be used to produce web thicknesses within the required tolerances. The use of steel masks in this study to produce up to three milled workpieces did not appear to affect web thickness significantly; measurements on random samples showed variations in web thickness of less than 0.003 inch from the first to the third sample. Detailed studies on this issue, along with the use of harder materials for masks, need to be addressed in future work.
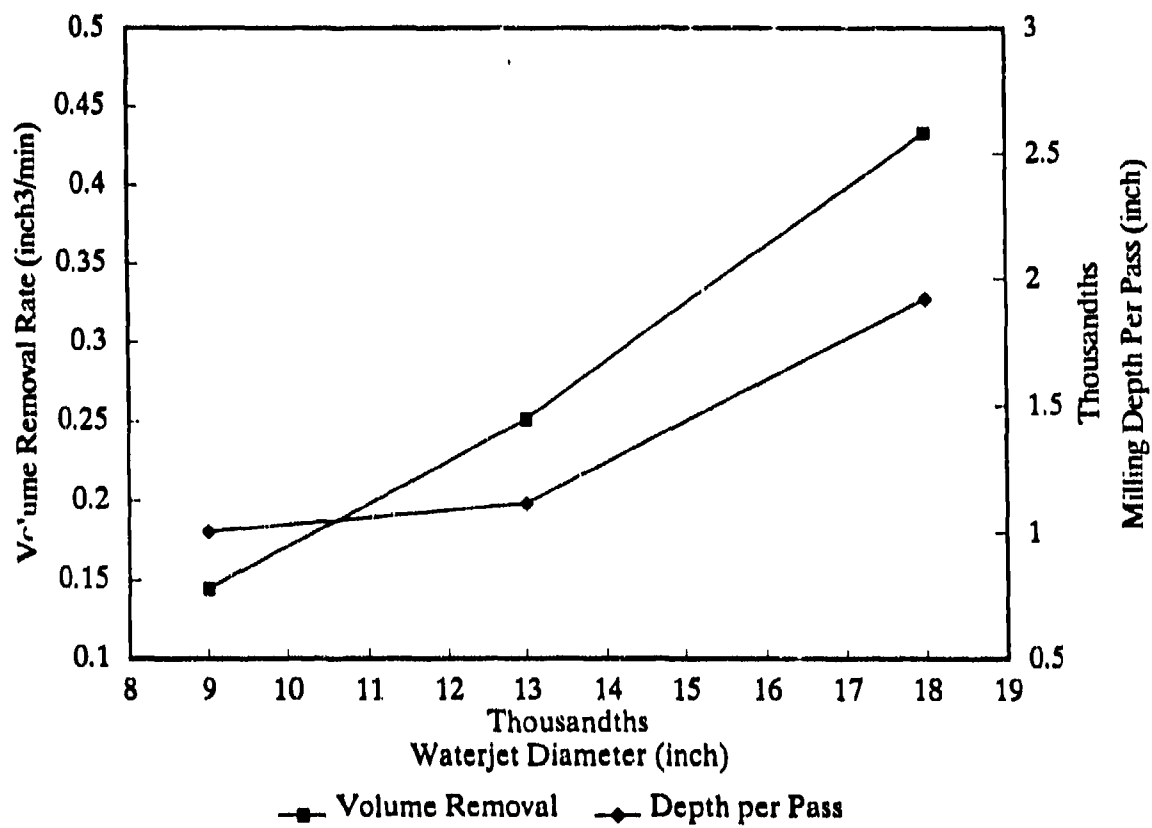
Figure 28. Effect of Waterjet Diameter on Volume Removal Rate and Milling Depth Per Pass. d_m = 0.047 inch, l_m = 3 inches, p = 50 ksi, gs mesh 100, m_a = 0.53 lb/min, n = 10.96 rps, inc = 0.6, u = 6.18 in/min (see appendix test numbers 31, 34-35)
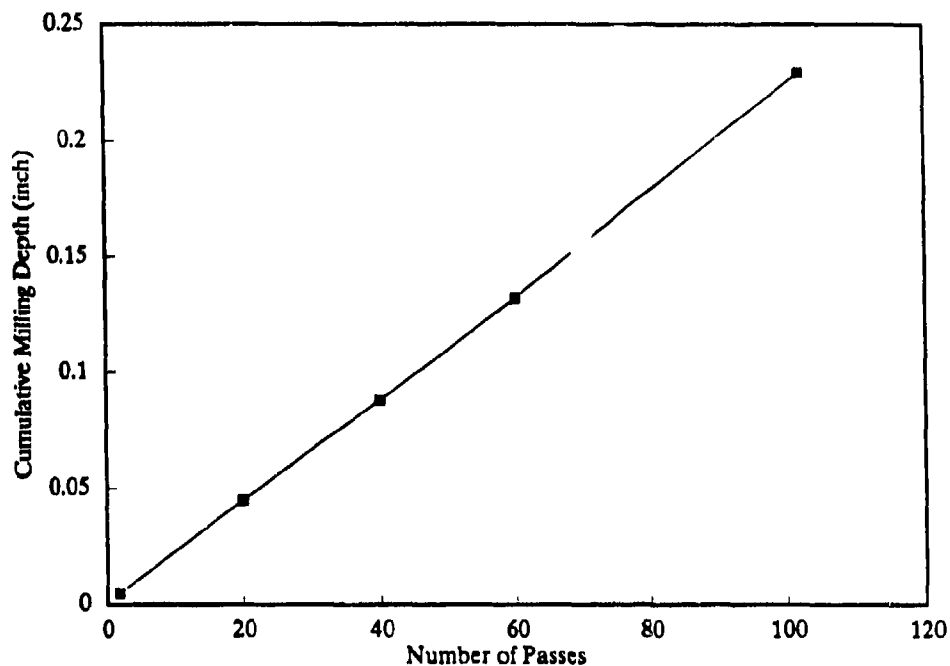
Figure 29a. Cumulative Milling Depth and Depth per Pass. d_m = 0.047 inch, l_m = 3 inches, d_n = 0.018 inch, p = 50 ksi, gs mesh 100, m_a = 1.30 lb/min, n = 10.96 rps, inc = 0.6, u = 6.18 in/min (see appendix test numbers 47-50)
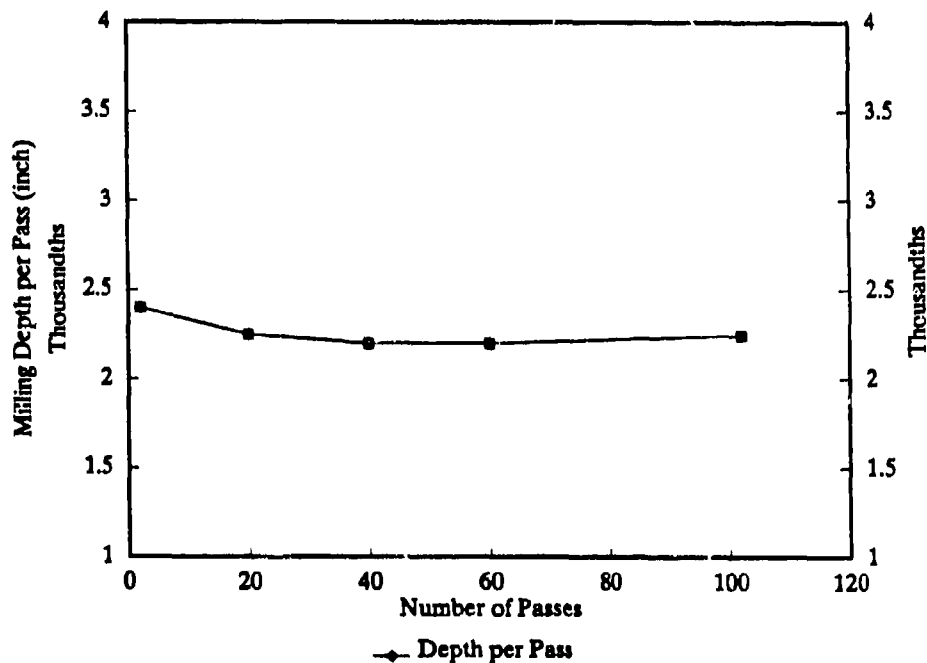
→ Depth per Pass

Figure 29b. Depth of Milling per Pass. d_m = 0.047 inch, l_m = 3 inches, d_n = 0.018 inch, p = 50 ksi, gs mesh 100, m_a = 1.30 lb/min, n = 10.96 rps, inc = 0.6, u = 6.18 in/min (see appendix test numbers 47-50)

Figure 30. Irregular Hole Boundary Due to Improper Masking

6. DIFFUSION BONDING

A number of industry sources were contacted and presented with the following question: Can a thin skin of sheet metal be diffusion-bonded to the outside of a 45-inch-diameter circular honeycomb isogrid panel? The skin material can be the same as the honeycomb material. The industry sources that we contacted included:

- Pressure Technology, Inc. (PTI)
- Howmet
- International Pressure Service, Inc. (IPS)
- Industrial Material Technology
- BeamAloy

Before presenting the findings, we will first describe the process of diffusion bonding. This process is a subset of hot isostatic pressing (HIP) technology, which uses high pressure and temperature to densify a powdered metal or plastic part or a previously sintered part.

The diffusion bonding procedure is used to enclose the part in a sealed bag or can that is evacuated of air. The part and can (or bag) are put into the furnace where they are exposed to high pressures at a temperature below the part's melting point. If the part is one that can be "HIPped" at low temperatures, such as plastics, a rubber bag is used and hydraulic fluid is used for pressurizing. If the part must be heated above the rubber's safe temperature, argon gas is used. Temperatures of 1,400 to 2,000°C and pressures of 15 to 30 ksi are used with the argon gas. Pressures up to 60 ksi are used with hydraulic fluid. The evacuation and pressurization process collapses the can completely over the part.

Diffusion bonding by this process was originally used to install cylinders over nuclear fuel rods. Not all parts have a shape that is conducive to this process, however; void spaces may collapse under the pressure. The can must completely conform to the outside surface of the part.

The cost of this process is about $2,000 to $2,600 per run. This does not include fabrication of the can. The furnace size varies from vendor to vendor. PTI's furnace is 16 inches in diameter and 44 inches long; IPS's furnace is about 60 inches long.

Based on our discussions with the industry sources, the following conclusions were made:

- This application is beyond the current state of the art in diffusion bonding.
- The shape of the isogrid honeycomb requires either an intricate can that conforms to the ribs and hollows or a can that spans the ribs without collapsing under pressure.
- The size of the part is larger than the furnaces surveyed.
- This application requires development efforts by an HIP company.

The industry sources listed above suggested the following alternatives:

- A brazing process submerged in heated flux
- Adhesive bonding

7. DEMONSTRATION MILLING OF ISOGRID PATTERNS

Isogrid milling tests were conducted using the most feasible approach to demonstrate the overall milling process. This approach involved the use of steel masks to AWJ machine the isogrid pattern in preformed aluminum tubes. The parameters for milling were selected from the previous tests. These are:

$$p = 50 \text{ ksi}$$
$$d_n = 0.018 \text{ inch}$$
$$d_m = 0.047 \text{ inch}$$
$$\text{garnet mesh} = 100$$
$$u = 8,000 \text{ in./min}$$
$$m_a = 1.3 \text{ lb/min}$$

Figure 31 shows plots of milling depth, milling depth per pass and volume removal rate for isogrid milling (see appendix, test numbers 51-54). The data were recorded by measuring the depth of milling after certain number of passes as shown in Figure 31. Figure 32 shows a milled sample and the steel mask used. The wear on the steel mask was less than one-third that of the aluminum; this implies that a steel mask can be used three times for isogrid milling.

Three rings were machined (using one mask) to produce 18 patterns such as the one shown in Figure 32a. In the demonstration milling tests, the depth of milling was frequently measured after every 10 or 20 passes. The measured depth was compared to the data given in Figure 31. All measured values fell within 0.003 inch of expected values, which is considered to be in close agreement with milling resolution (depth per pass).

Figure 33 shows the steel masks mounted on the inside of a tube. Obviously, a mask that was in the form of a complete cylinder could have been used. Figure 34 shows the milled ring after removing the masks.

Isogrid patterns were inspected for surface finish and uniformity of depth. No efforts were conducted in this study to control the surface finish, as efforts were mainly focused on controlling the depth of milling. Figure 35 shows a profilometer plot of a representative milled surface. Observe that the surface is uniform in depth and that the roughness contour is regular.

A number of milled aluminum sections were inspected for milling depth uniformity. Measurements were conducted at various locations, as shown in Figure 36. Eleven radial locations were selected to measure the skin thickness on a milled aluminum tube to a nominal skin thickness of 0.092 inch. At every radial location, two measurements were taken using a micrometer with ball points. The aluminum thickness was also measured as a reference check to ensure the accuracy of the data. The measured skin thickness data are shown in Table 1.
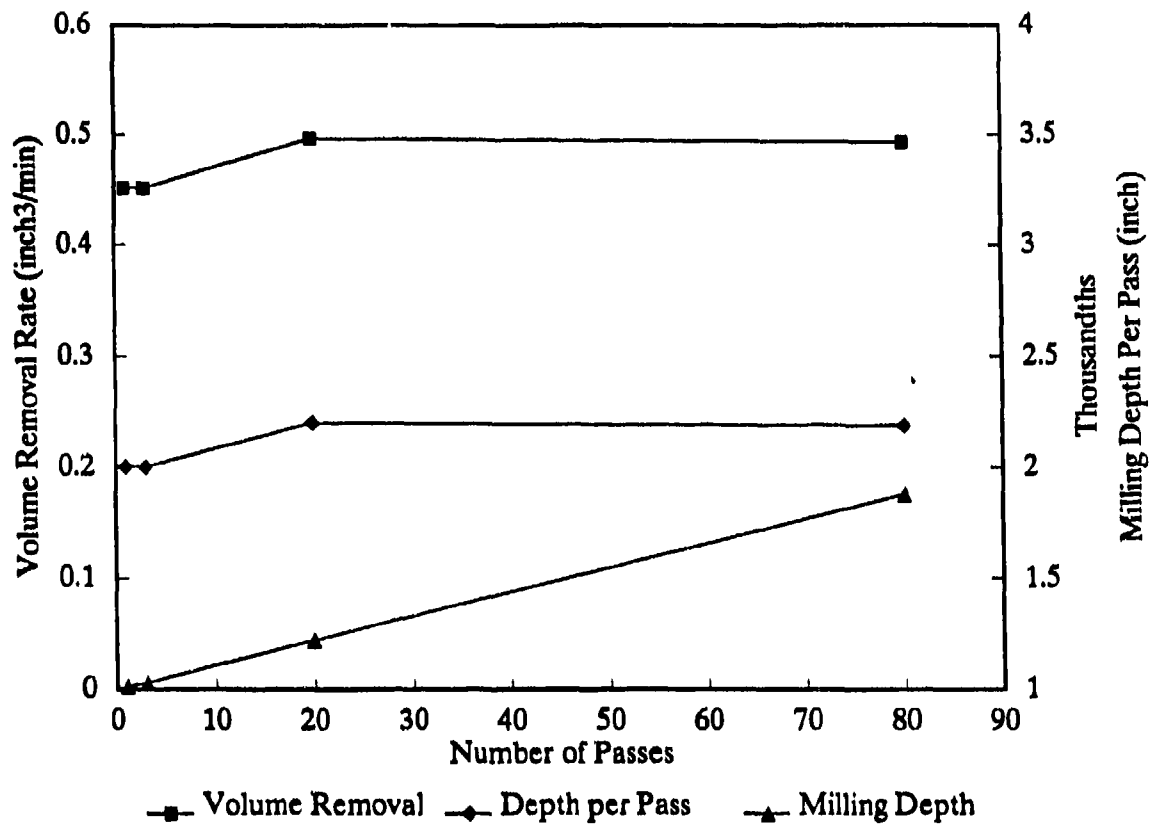
Figure 31. Volume Removal Rate and Depth of Milling Progression with Number of Passes. (see appendix test numbers 51-54)
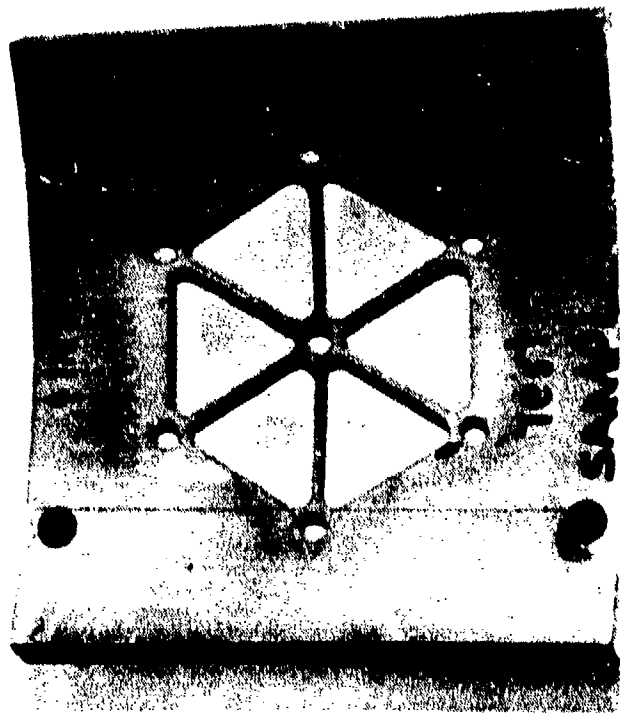
b. Steel mask

a. Milled isogrid pattern
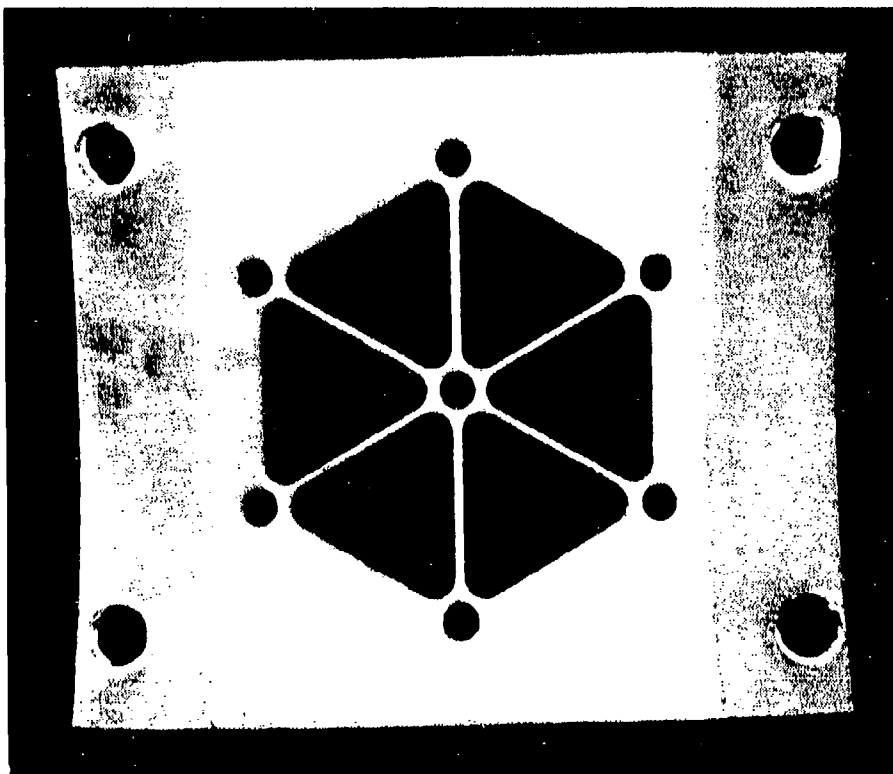
Figure 32. AWJ-Milled Isogrid Pattern and Steel Mask
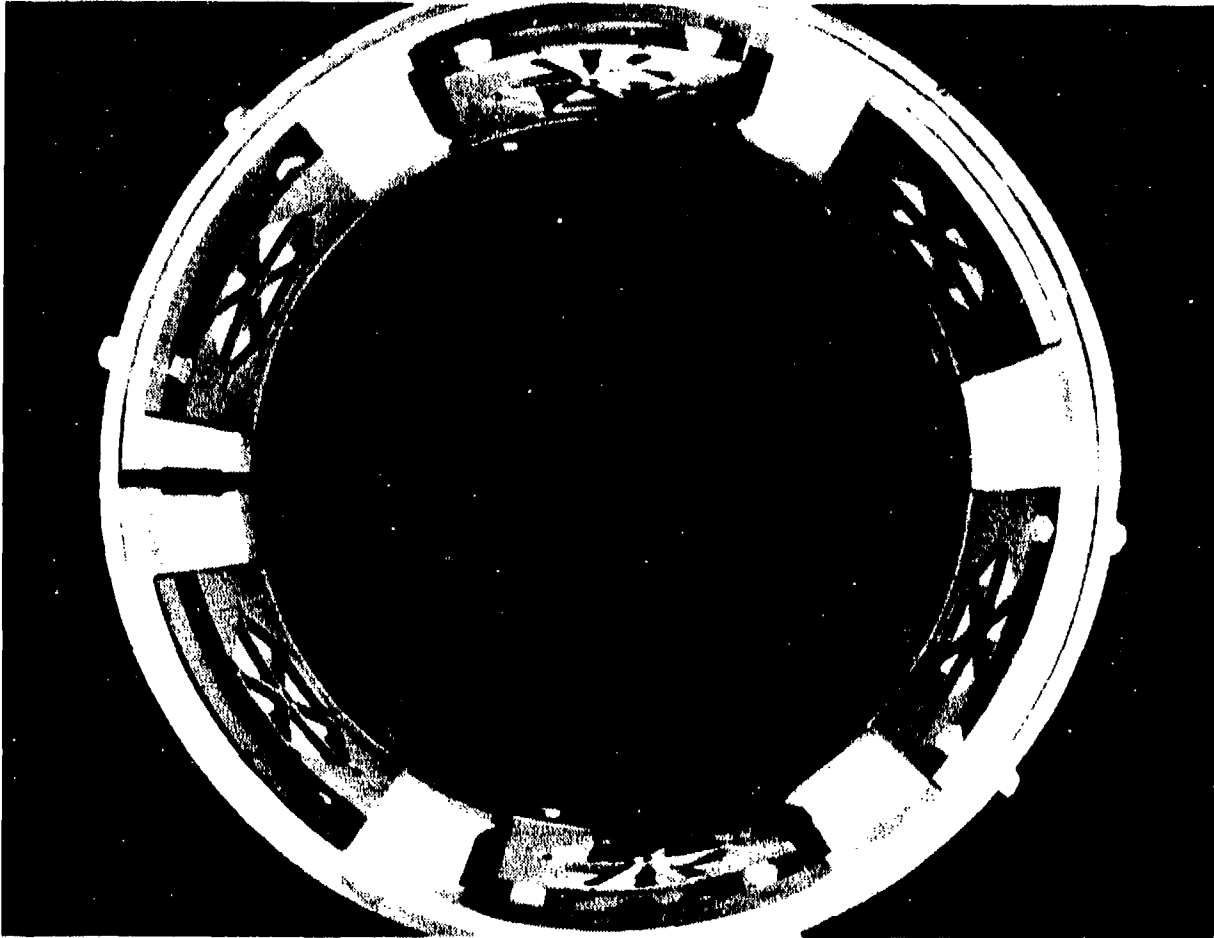
Figure 33.   Multiple Isogrid Patterns Milled on Inside of Tube
Using a Number of Masks
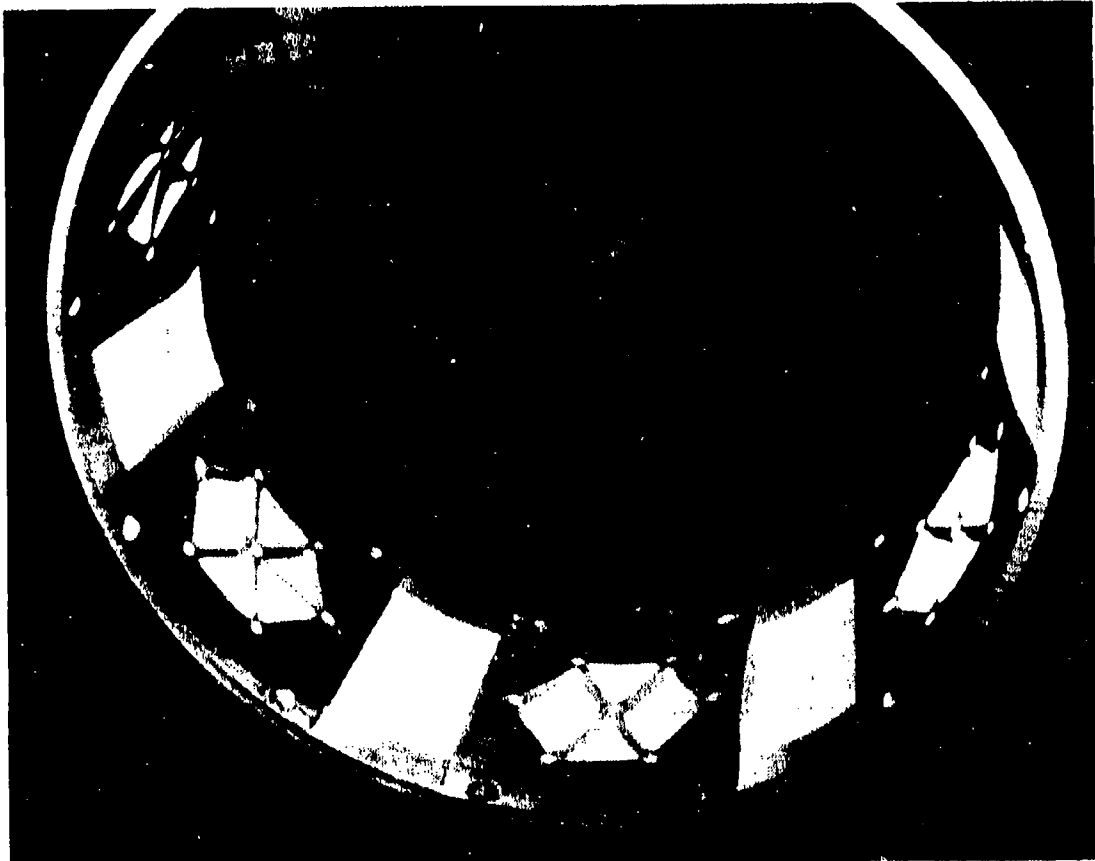
Figure 34.   Isogrid Pattern Milled on Inside of Tube
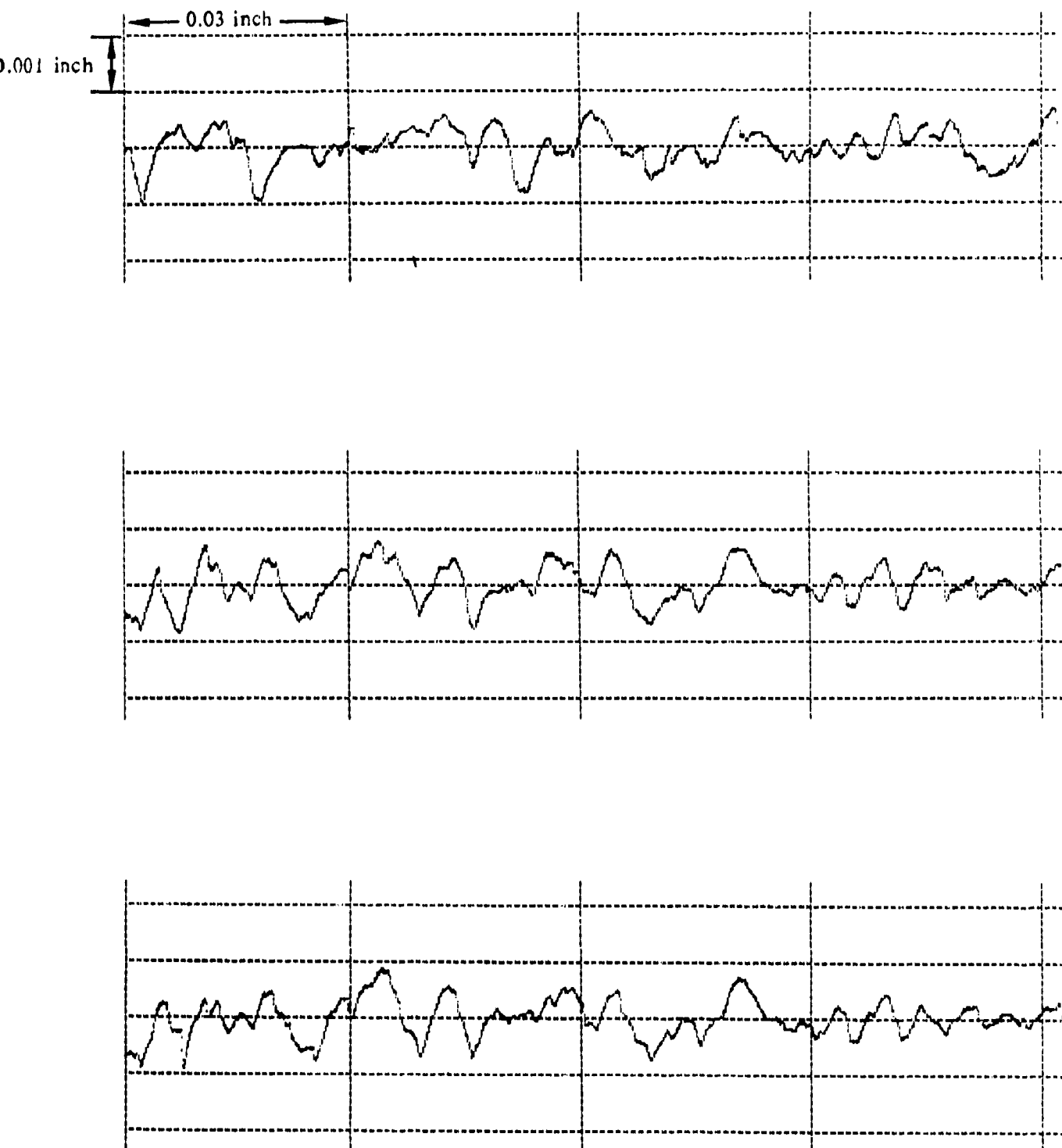
Figure 35. Surface Finish Profile of a Typical Milled Surface at Three Different Locations. The average roughness in 541 microinches

AXIAL POSITIONS

RADIAL POSITIONS

INSPECTION LOCATIONS
FOR MILLED TUBE

INSPECTION LOCATIONS
FOR AN ISOGRID PATTERN

INSPECTION LOCATIONS
INSIDE A TRIANGLE
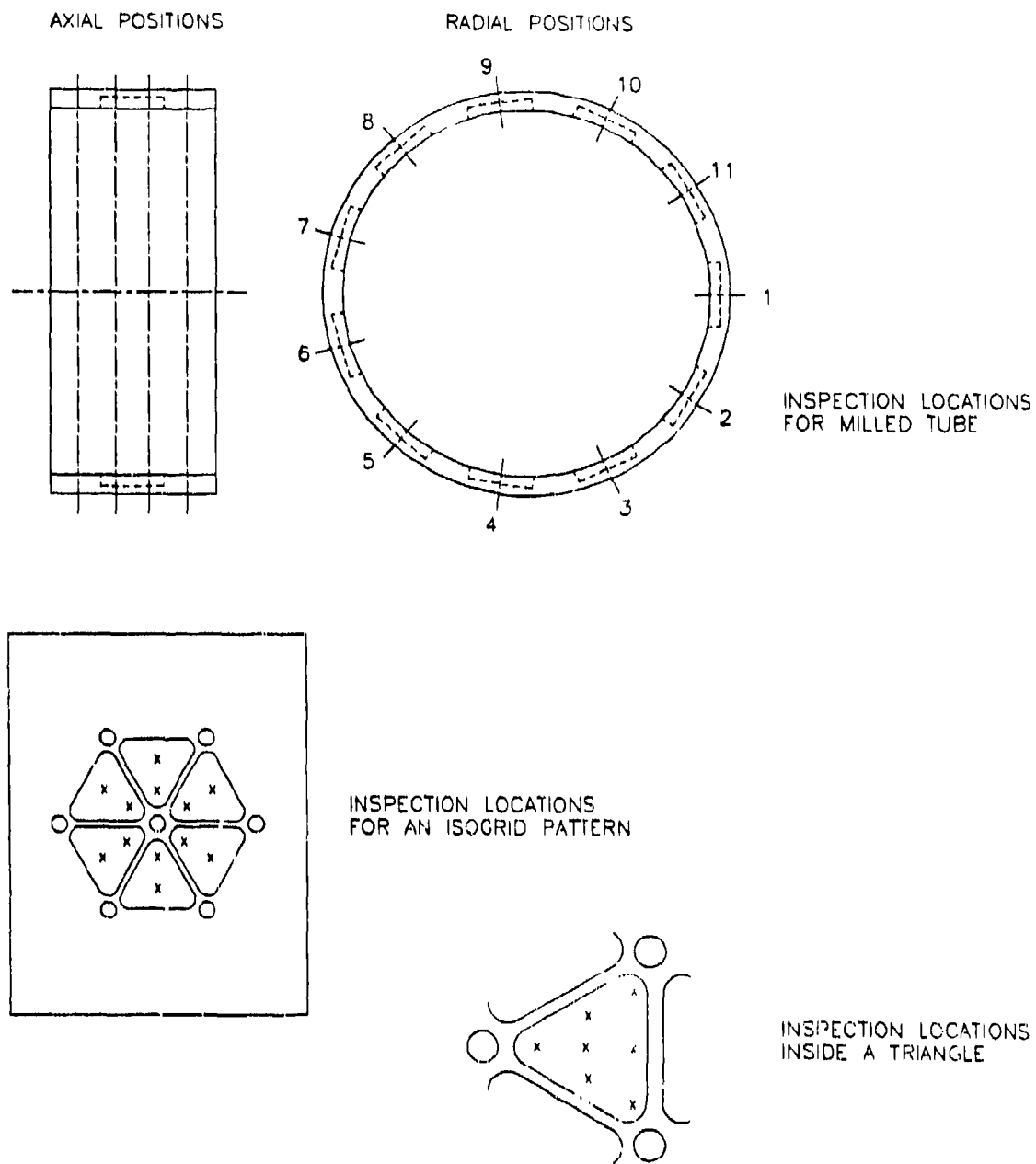
Figure 36.   Inspection Locations for Milled Sections

Table 1. Skin Thickness Uniformity on an AWJ-Milled Aluminum Tube

Radial Location	Skin Thickness Location 1	Skin Thickness Location 2
1	0.092	0.093
2	0.093	0.094
3	0.094	0.094
4	0.092	0.093
5	0.093	0.093
6	0.093	0.093
7	0.090	0.091
8	0.092	0.092
9	0.093	0.092
10	0.095	0.094
11	0.093	0.093

Average thickness = 0.093
Standard deviation = 0.001

Skin thickness measurements were also recorded at 12 locations inside two six-way isogrid patterns milled on different tubes. The inspection data are shown in Table 2.

Another set of skin thickness measurements at seven locations inside a triangle as shown in Figure 36. Two samples were used for this test, and the data are given in Table 3.

It can be seen from the data in Tables 1 through 3 that milling depth can be controlled to approximately 0.001 inch. Standard deviation data on milling depth showed a maximum deviation of 0.0015 inch. Process refinement by improved control over the parameters and optimization will result in improved uniformity.

Table 2. Skin Thickness Measurements at 12 Locations
Inside Six-way Structure (two each triangle)

Location	Test Sample 1	Test Sample 2
1	0.051	0.036
2	0.051	0.036
3	0.054	0.034
4	0.052	0.034
5	0.054	0.036
6	0.053	0.034
7	0.053	0.035
8	0.053	0.036
9	0.054	0.035
10	0.051	0.034
11	0.053	0.033
12	0.051	0.035
Average Thickness	0.052	0.035
Standard Deviation	0.001	0.001

Table 3. Skin Thickness Measurements at Seven Locations
Inside One Triangle

Location	Test Sample 1	Test Sample 2
1	0.052	0.035
2	0.052	0.034
3	0.049	0.035
4	0.051	0.033
5	0.051	0.034
6	0.052	0.036
7	0.053	0.033
Average Thickness	0.051	0.034
Standard Deviation	0.001	0.001

8. ECONOMIC ANALYSIS

Here, we present a simple economic analysis to estimate the approximate cost of AWJ milling of isogrid structures. A detailed analysis and cost optimization will be conducted in Phase II and will include addressing the design and manufacturing of a machining center.

The cost analysis is based on a machining center consisting of the following subsystems:

- High-pressure pumping system
- Nozzle and workpiece manipulator system(s)
- Nozzle and abrasive feed system
- Sensors and controls
- Waste handling system

The high pressure pumping system should be sufficient to at least power a single nozzle. A typical nozzle used in this study operates at 45 ksi and 0.75 gal/min of water. This requires about 28 horsepower, which is well within the operating range of commercially available pumping units. The cost of high-pressure pumps varies between $30,000 and $80,000, depending on the desired degree of control, pressures, and flow rates.

The manipulator for the nozzle and workpiece uses a rotating workpiece (which is a cylinder) and axially moves the nozzle inside this cylinder at the proper standoff distance. This system can be used for milling and will also be used for cutting the mask, which requires that the part rotation unit can be programmed for position control. There are alternatives to this approach which, again, will be addressed in detail in another study. For the purpose of this cost analysis, it will be assumed that the manipulator system will cost $300,000.

The nozzle and abrasive feed system will be typical of current commercially available hardware. A typical price for a complete unit is $13,000.

Sensors and controls represent an important subsystem which can be of varying degrees of complexity. Process parameters need to be accurately monitored and controlled for precision machining. Additionally, the machining results need to be frequently inspected. It will be assumed in this study that the cost of the sensors and controls is $50,000.

The waste recovery system will consist of a sludge pump and a settling container. The water, abrasives, and cutting debris will be transported from the cutting area to the settling tank via hoses. The cost for this system is assumed to be $30,000.

Thus, the total capital cost for an AWJ machining center for isogrid milling will be assumed to be $500,000.

The hourly costs of system operation are as follows:

Capital Equipment:	$48
Maintenance:	$5
Consumables (orifice, tubes, abrasives, etc.):	$20
Power (based on 75 horsepower):	$5
Operator	$15
TOTAL HOURLY COST:	$93

Here, the hourly cost of capital equipment is based on the following assumptions: 7-year lifetime, 8 hr/day operation, 10% interest rate, and zero residual (scrap) value.

The machining process for an isogrid structure will consist of steel mask cutting and aluminum skirt milling. The machining time will be estimated for an example case. In this case, an isogrid pattern in a 36-inch inside diameter aluminum tube with a length of 12 inches will be considered. The total linear inches of cutting a steel mask is estimated at 5,940 inches. This was calculated based on the geometry given in Figure 1. A steel mask made out of a 36-inch outside diameter tube with 0.25-inch thickness and 12-inch height will require a total of about 10.1 hours of cutting. The cutting speed for steel used in this estimation is 10 in./min, although this speed can be increased to 20 in./min with multiple or more powerful jets.

The milling time can be calculated simply based on the total volume to be removed and the volume removal rate data generated in this study. The volume to be swept is $\pi*4*D*L*h$. For our example, the length L is 12 inches, the diameter D is 36 inches, and the depth of milling h will be 0.24 inch. Thus, the total volume is approximately 362 in.^{3} Assuming that a single jet will be used, the volume removal rate will be about 0.5 in.^{3}/min. This leads to a total milling time of about 10.86 hours. The total AWJ machining time for an isogrid tube (36-inch inside diameter, 12 inches long) is then about 21 hours, which includes steel mask cutting time and aluminum milling.

One mask, however, can effectively be used three times. For the above example, a 36-inch-long section will require only one mask (12 inches long) to be indexed axially to mill three 12-inch-long sections. The total machining time for a 36-inch-long skirt will be 10.86 * 3 + 10.1 = 42.7 hours.

This example is shown in Table 4, which also shows additional data on the milling time of isogrid skirts. In this table, N_j is the number of jets to be used, D is the inside diameter to be milled, and L is the height of the tubular skirt. The mask cutting time T_c is given for steel while the milling time T_m is given for aluminum. For this simple analysis, the total time T_t is calculated by adding one-third of the steel mask cutting time to the milling time.

Table 4. Mask Cutting and Isogrid Milling Times

N_j	D (inch)	L (inch)	T_c (hr)	T_m (hr)	T_t (hr)	N_j	D (inch)	L (inch)	T_c (hr)	T_m (hr)	T_t (hr)
1	36	12	10.1	10.9	14.2	2	36	36	15.2	16.3	21.3
1	42	12	11.8	12.7	16.6	2	42	36	17.7	19.0	24.9
1	48	12	13.5	14.5	19.0	2	48	36	20.2	21.7	28.4
1	56	12	15.7	16.9	22.1	2	56	36	23.6	25.3	33.2
1	36	24	20.2	21.7	28.4	2	36	48	20.2	21.7	28.4
1	48	24	26.9	28.9	37.9	2	48	48	26.9	28.9	37.9
1	48	24	26.9	28.9	37.9	2	48	48	26.9	28.9	37.9
1	56	24	31.4	33.8	44.2	2	56	48	31.4	33.8	44.2
1	36	36	30.3	32.6	42.7	3	36	12	3.4	3.6	4.7
1	42	36	35.4	38.0	49.8	3	42	12	3.9	4.2	5.5
1	48	36	40.4	43.4	56.9	3	48	12	4.5	4.8	6.3
1	56	36	47.1	50.6	66.4	3	56	12	5.2	5.6	7.4
1	36	48	40.4	43.4	56.9	3	36	24	6.7	7.2	9.5
1	48	48	53.9	57.9	75.8	3	48	24	9.0	9.6	12.6
1	48	48	53.9	57.9	75.8	3	48	24	9.0	9.6	12.6
1	56	48	62.9	67.5	88.5	3	56	24	10.5	11.3	14.7
2	36	12	5.1	5.4	7.1	3	36	36	10.1	10.9	14.2
2	42	12	5.9	6.3	8.3	3	42	36	11.8	12.7	16.6
2	48	12	6.7	7.2	9.5	3	48	36	13.5	14.5	19.0
2	56	12	7.9	8.4	11.1	3	56	36	15.7	16.9	22.1
2	36	24	10.1	10.9	14.2	3	36	48	13.5	14.5	19.0
2	48	24	13.5	14.5	19.0	3	48	48	18.0	19.3	25.3
2	48	24	13.5	14.5	19.0	3	48	48	18.0	19.3	25.3
2	56	24	15.7	16.9	22.1	3	56	48	21.0	22.5	29.5

The above examples suggest that there may be an optimum mask length based on the total length of the skirt. For example, a mask length of 18 inches may be more economical than a shorter mask. Also, a harder mask material such as tungsten carbide, which may last over 30 times as long as steel, may be more economical even though more expensive initially. Additionally, mask machining may be done by laser if that method is more economical. Another optimization issue is related to the use of multiple jets rather than a single jet, which will reduce the machining time in direct proportions. All these factors need to be addressed in a detailed optimization effort.

Let us assume now that a 36-inch-long skirt with a 36-inch inside diameter needs to be milled with the isogrid pattern. The total machining time will be 42.7 hours, as determined earlier. The hourly cost of equipment operation is $93, as approximated above. With overhead, it can be assumed that the total hourly cost is approximately $279 based on a total multiple of 3. Accordingly, the total cost of machining will be 42.7 × 279 = $11,913. This cost can be reduced significantly through optimization as discussed above.

9. CONCLUSIONS AND RECOMMENDATIONS

The following conclusions can be made based on the results of the study presented in this report:

- Abrasive-waterjets have been demonstrated to be capable of milling isogrid patterns precisely in aluminum.
- This feasibility investigation indicated that cavities can be AWJ-milled in aluminum to a uniformity of 0.001 inch. Improved surface uniformity can be achieved with further process refinement.
- Surface finish improvement was not attempted in this phase. It is recommended that this effort be addressed in future studies.
- The AWJ milling process can be achieved on curved surfaces on the inside of tubes.
- The AWJ isogrid machining process includes mask cutting, which can be achieved using the same AWJ nozzle.
- For example, the total machining time of a 48-inch-diameter, 12-inch-long skirt is estimated at 6.3 hours if three jets are used.
- Aluminum through-cutting of isogrid patterns can be achieved at high rates (exceeding 30 in./min) on curved surfaces (from the inside or outside of a tube). The cutting time for a 48-inch-diameter, 12-inch-long skirt is estimated as 4.5 hours with a single jet.
- Diffusion bonding of thin aluminum skins on a machined skirt appears to be beyond the current state-of-the art.
- The use of the "mask and mill" approach is the most promising of the AWJ milling methods.
- Optimization of the AWJ milling process and improved masking techniques are efforts that need to be addressed in more detail.
- The AWJ milling process is not limited to specific shapes as in conventional milling. Consequently, more efficient isogrid shapes can be machined to reduce parasitic weight. Also, the AWJ process presents no limitation on material.

REFERENCES

Hashish, M. (1989b) "A Model of Abrasive-Waterjet Machining," Transactions of the ASME, *Journal of Materials and Technology*, Vol. 111, pp. 154-162.

Hashish, M. (1988) "Turning, Milling, and Drilling with Abrasive-Waterjets," *Proceedings of the 9th International Symposium on Jet Cutting Technology*, BHRA, Sendi, Japan, October, pp. 113-131.

APPENDIX

SPREADSHEET PRINTOUT OF EXPERIMENTAL DATA

The symbols used on the following pages are explained below:

No	=	test number
dm	=	diameter of mixing tube
lm	=	length of mixing tube
dn	=	waterjet orifice diameter
p	=	pressure
gs	=	garnet sand
ma	=	abrasive flow rate
Vt	=	traverse rate
N	=	drum rotational speed per second
inc	=	ratio of cross-feed increment to mixing tube diameter
i	=	increment of AWJ cross-feed
u	=	cross-feed rate
sp	=	motor setting in counts per second
Np-cc	=	number of passes counterclockwise
Np-c	=	number of passes clockwise
sod	=	standoff distance
area	=	milling area
volume	=	volume removed
av. h	=	average depth
h/pss	=	average depth of milling per pass
vol rate	=	volume removal rate

ABRASIVE / **WEIGHT**

No	da inch	lm inch	dh inch	p ksi	type	size	m lb/min	valve setting	Vt in/mi	N rps	inc i/da	i inch	u in/mi	sp cm/sec	Np-cc pass	Np-c pass	sod inch	before grams	after grams	loss grams	area inch2	volume inch3	av. h inch	h/pss inch	vol rate inch3/min
1	0.047	3	0.013	45	gs	100	0.53	3.25	4000	5.48	0.4	0.019	2.06	2747	1	0	0.925	267.00	266.85	0.15	1.060	0.003	0.0029	0.0029	0.2166
2	0.047	3	0.013	45	gs	100	0.53	3.25	4000	5.48	0.4	0.019	2.06	2747	20	0	0.925	266.85	264.00	2.85	1.060	0.058	0.0547	0.0027	0.2057
3i	0.047	3	0.013	45	gs	100	0.53	3.25	4000	5.48	0.4	0.019	2.06	2747	20	20	0.3	404.00	383.00	21.00	3.400	0.427	0.1256	0.0031	0.2362
EFFECT OF OVERLAP ON .013/.047																									
8	0.047	3	0.013	45	gs	100	0.53	3.25	4000	5.48	0.2	0.009	1.03	1373	20	0	0.3	165.64	161.80	3.84	0.885	0.078	0.0882	0.0044	0.1659
7	0.047	3	0.013	45	gs	100	0.53	3.25	4000	5.48	0.4	0.019	2.06	2747	20	0	0.3	167.79	165.64	2.15	0.885	0.044	0.0494	0.0025	0.1857
4	0.047	3	0.013	45	gs	100	0.53	3.25	4000	5.48	0.6	0.028	3.09	4120	20	0	0.3	160.48	158.90	1.58	0.885	0.032	0.0363	0.0018	0.2047
5	0.047	3	0.013	45	gs	100	0.53	3.25	4000	5.48	0.8	0.038	4.12	5494	20	0	0.3	158.90	157.70	1.20	0.885	0.024	0.0276	0.0014	0.2073
6	0.047	3	0.013	45	gs	100	0.53	3.25	4000	5.48	1.0	0.047	5.15	6867	20	0	0.3	157.81	156.96	0.85	0.885	0.017	0.0195	0.0010	0.1836
EFFECT OF OVERLAP ON .013/.062																									
9	0.062	3	0.013	45	gs	100	0.53	3.25	4000	5.48	0.2	0.012	1.36	1812	20	0	0.3	162.06	159.16	2.90	0.885	0.059	0.0666	0.0033	0.1652
10	0.062	3	0.013	45	gs	100	0.53	3.25	4000	5.48	0.4	0.025	2.72	3623	20	0	0.3	164.10	162.52	1.58	0.885	0.032	0.0363	0.0018	0.1801
11	0.062	3	0.013	45	gs	100	0.53	3.25	4000	5.48	0.6	0.037	4.08	5435	20	0	0.3	162.52	161.41	1.11	0.885	0.023	0.0255	0.0013	0.1897
12	0.062	3	0.013	45	gs	100	0.53	3.25	4000	5.48	0.8	0.050	5.44	7247	20	0	0.3	161.41	160.57	0.84	0.885	0.017	0.0193	0.0010	0.1914
13	0.062	3	0.013	45	gs	100	0.53	3.25	4000	5.48	1.0	0.062	6.79	9059	20	0	0.3	164.70	164.10	0.60	0.885	0.012	0.0138	0.0007	0.1709
EFFECT OF OVERLAP ON .013/.093																									
14	0.093	3	0.013	45	gs	100	0.53	3.25	4000	5.48	0.2	0.019	2.04	2718	20	0	0.3	164.10	162.42	1.68	0.885	0.034	0.0396	0.0019	0.1435
15	0.093	3	0.013	45	gs	100	0.53	3.25	4000	5.48	0.4	0.037	4.08	5435	20	0	0.3	162.30	161.44	0.86	0.885	0.017	0.0198	0.0010	0.1470
16	0.093	3	0.013	45	gs	100	0.53	3.25	4000	5.48	0.6	0.056	6.11	8153	20	0	0.3	173.12	172.55	0.57	0.885	0.012	0.0131	0.0007	0.1461
17	0.093	3	0.013	45	gs	100	0.53	3.25	4000	5.48	0.8	0.074	8.15	10870	20	0	0.3	172.55	172.13	0.42	0.885	0.009	0.0096	0.0005	0.1436
18	0.093	3	0.013	45	gs	100	0.53	3.25	4000	5.48	1.0	0.093	10.19	13588	40	0	0.3	172.13	171.48	0.65	0.885	0.013	0.0149	0.0004	0.1389
EFFECT OF STAND OFF DISTANCE																									
23	0.047	3	0.013	45	gs	100	0.53	3.25	4000	5.48	0.6	0.028	3.09	4120	20	0	0.3	172.43	170.76	1.67	0.885	0.034	0.0384	0.0019	0.2164
19	0.047	3	0.013	45	gs	100	0.53	3.25	4000	5.48	0.6	0.028	3.09	4120	20	0	0.5	165.41	163.78	1.63	0.885	0.033	0.0374	0.0019	0.2112
20	0.047	3	0.013	45	gs	100	0.53	3.25	4000	5.48	0.6	0.028	3.09	4120	20	0	0.6	163.61	161.77	1.64	0.885	0.033	0.0377	0.0019	0.2125
21	0.047	3	0.013	45	gs	100	0.53	3.25	4000	5.48	0.6	0.028	3.09	4120	20	0	0.9	175.82	174.17	1.65	0.885	0.034	0.0379	0.0019	0.2138
22	0.047	3	0.013	45	gs	100	0.53	3.25	4000	5.48	0.6	0.028	3.09	4120	20	0	1.2	176.17	172.54	1.63	0.885	0.033	0.0374	0.0019	0.2112
EFFECT OF TRAVERSE RATE																									
24	0.047	3	0.013	45	gs	100	0.53	3.25	1000	1.37	0.6	0.028	0.77	1030	10	0	0.6	164.20	160.70	3.50	0.885	0.071	0.0804	0.0080	0.2268
25	0.047	3	0.013	45	gs	100	0.53	3.25	2000	2.74	0.6	0.028	1.55	2060	10	0	0.6	160.55	158.88	1.67	0.885	0.034	0.0384	0.0038	0.2164
20	0.047	3	0.013	45	gs	100	0.53	3.25	4000	5.48	0.6	0.028	3.09	4120	20	0	0.6	163.41	161.77	1.64	0.885	0.033	0.0377	0.0019	0.2125
26	0.047	3	0.013	45	gs	100	0.53	3.25	8000	10.96	0.6	0.028	6.18	8241	40	0	0.6	158.88	157.97	0.91	0.885	0.019	0.0209	0.0010	0.2358
27	0.047	3	0.013	45	gs	100	0.53	3.25	12000	16.44	0.6	0.028	9.27	12361	80	0	0.6	166.32	163.94	2.38	0.885	0.048	0.0547	0.0007	0.2313

ABRASIVE   WEIGHT

No	dn inch	ln inch	dn inch	p tsi	type	size	na lb/min	valve setting	Vt in/mi	N rps	inc i/dm	i inch	u in/mi	sp cn/sec	lip-cc pass	lip-c pass	sod inch	before grams	after grams	loss grams	area inch2	volume inch3	av. h inch	h/pss inch	vol rate inch3/min
EFFECT OF PARTICLE SIZE																									
28	0.047	3	0.013	45	gs	150	0.53	3.25	8000	10.96	0.6	0.028	6.18	8241	40	0	0.6	163.94	162.85	1.09	0.885	0.022	0.0250	0.0006	0.1412
26	0.047	3	0.013	45	gs	100	0.53	3.25	8000	10.96	0.6	0.028	6.18	8241	20	0	0.6	158.88	157.97	0.91	0.885	0.019	0.0209	0.0010	0.2358
29	0.047	3	0.013	45	gs	80	0.53	3.00	8000	10.96	0.6	0.028	6.18	8241	40	0	0.6	162.85	161.03	1.82	0.885	0.037	0.0418	0.0010	0.2358
30	0.047	3	0.013	45	gs	60	0.53	3.00	8000	10.96	0.6	0.028	6.18	8241	40	0	0.6	175.24	173.42	1.82	0.885	0.037	0.0418	0.0010	0.2358
EFFECT OF PRESSURE																									
31	0.047	3	0.013	50	gs	100	0.53	3.25	8000	10.96	0.6	0.028	6.18	8241	40	0	0.6	173.42	171.48	1.94	0.885	0.039	0.0446	0.0011	0.2514
26	0.047	3	0.013	45	gs	100	0.53	3.25	8000	10.96	0.6	0.028	6.18	8241	20	0	0.6	158.88	157.97	0.91	0.885	0.019	0.0209	0.0010	0.2358
32	0.047	3	0.013	40	gs	100	0.53	3.25	8000	10.96	0.6	0.028	6.18	8241	80	0	0.6	171.48	168.80	2.68	0.885	0.055	0.0616	0.0008	0.1736
33	0.047	3	0.013	30	gs	100	0.53	3.25	8000	10.96	0.6	0.028	6.18	8241	80	0	0.6	172.72	170.97	1.75	0.885	0.036	0.0402	0.0005	0.1134
EFFECT OF NOZZLE COMBINATION																									
34	0.030	3	0.009	50	gs	100	0.35	2.75	8000	10.96	0.6	0.018	3.94	5260	80	0	0.6	164.29	160.80	3.49	0.885	0.071	0.0802	0.0010	0.1443
31	0.047	3	0.013	50	gs	100	0.53	3.25	8000	10.96	0.6	0.028	6.18	8241	40	0	0.6	173.42	171.48	1.94	0.885	0.039	0.0446	0.0011	0.2514
35	0.047	3	0.018	50	gs	100	1.30	4.50	8000	10.96	0.6	0.028	6.18	8241	80	0	0.6	170.97	164.29	6.68	0.885	0.136	0.1535	0.0019	0.4328
EFFECT OF ABRASIVE FLOW RATE																									
36	0.062	3	0.018	50	gs	100	0.35	2.75	8000	10.96	0.6	0.037	8.15	10870	80	0	0.6	178.25	175.33	2.92	0.885	0.059	0.0671	0.0008	0.2696
37	0.062	3	0.018	50	gs	100	0.53	3.25	8000	10.96	0.6	0.037	8.15	10870	80	0	0.6	175.33	171.72	3.61	0.885	0.073	0.0829	0.0010	0.3085
38	0.062	3	0.018	50	gs	100	0.75	3.75	8000	10.96	0.6	0.037	8.15	10870	80	0	0.6	171.72	167.36	4.36	0.885	0.089	0.1002	0.0013	0.3726
39	0.062	3	0.018	50	gs	100	1.00	4.00	8000	10.96	0.6	0.037	8.15	10870	80	0	0.6	175.10	170.37	4.73	0.885	0.096	0.1087	0.0014	0.4043
41	0.062	3	0.018	50	gs	100	1.55	5.00	8000	10.96	0.6	0.037	8.15	10870	80	0	0.6	168.62	163.39	5.23	0.885	0.106	0.1202	0.0015	0.4470
42	0.062	3	0.018	50	gs	100	1.30	4.50	8000	10.96	0.6	0.037	8.15	10870	236	0	0.6	174.43	0.00	-	0.885	-	-	-	-
MILLING TO PREDICTED DEPTH																									
43	0.047	3	0.018	50	gs	100	1.30	4.50	8000	10.96	0.6	0.028	6.18	8241	40	0	0.6	0.00	0.00	-	0.885	-	0.0200	0.0005	0.1128
44	0.047	3	0.018	50	gs	100	1.30	4.50	8000	10.96	0.6	0.028	6.18	8241	40	0	0.6	0.00	0.00	-	0.885	-	0.0400	0.0010	0.2256
45	0.047	3	0.018	50	gs	100	1.30	4.50	8000	10.96	0.6	0.028	6.18	8241	20	0	0.6	0.00	0.00	-	0.885	-	0.0350	0.0018	0.3948
46	0.047	3	0.018	50	gs	100	1.30	4.50	8000	10.96	0.6	0.028	6.18	8241	20	0	0.6	0.00	0.00	-	0.885	-	0.0430	0.0022	0.4850
50	0.047	3	0.018	50	gs	100	1.30	4.50	8000	10.96	0.6	0.028	6.18	8241	2	0	0.6	0.00	0.00	-	0.885	-	0.0048	0.0024	0.5414
49	0.047	3	0.018	50	gs	100	1.30	4.50	8000	10.96	0.6	0.028	6.18	8241	20	0	0.6	0.00	0.00	-	0.885	-	0.0450	0.0023	0.5076
47	0.047	3	0.018	50	gs	100	1.30	4.50	8000	10.96	0.6	0.028	6.18	8241	40	0	0.6	0.00	0.00	-	0.885	-	0.0880	0.0022	0.4963
48	0.047	3	0.018	50	gs	100	1.30	4.50	8000	10.96	0.6	0.028	6.18	8241	60	0	0.6	0.00	0.00	-	0.885	-	0.1320	0.0022	0.4963
A	0.047	3	0.018	50	gs	100	1.30	4.50	8000	10.96	0.6	0.028	6.18	8241	102	0	0.6	0.00	0.00	-	0.885	-	0.2290	0.0022	0.5065
ISOGRID PATTERN TO DEPTH																									
51	0.047	3	0.018	50	gs	100	1.30	4.50	8000	10.96	0.6	0.028	6.18	8241	80	0	0.6	0.00	0.00	-	0.885	-	0.1750	0.0022	0.4935
52	0.047	3	0.018	50	gs	100	1.30	4.50	8000	10.96	0.6	0.028	6.18	8241	20	0	0.6	0.00	0.00	-	0.885	-	0.0440	0.0022	0.4963
53	0.047	3	0.018	50	gs	100	1.30	4.50	8000	10.96	0.6	0.028	6.18	8241	3	0	0.6	0.00	0.00	-	0.885	-	0.0060	0.0020	0.4512
54	0.047	3	0.018	50	gs	100	1.30	4.50	8000	10.96	0.6	0.028	6.18	8241	1	0	0.6	0.00	0.00	-	0.885	-	0.0020	0.0020	0.4512
CARBIDE MASKED HOLES																									
55	0.047	3	0.018	50	gr	100	1.30	4.50	8000	10.96	0.6	0.028	6.18	8241	50	0	0.6	0.00	0.00	-	0.885	-	0.000	0.0000	0.0000
56	0.047	3	0.018	50	gs	100	1.30	4.50	8000	10.96	0.6	0.028	6.18	8241	40	0	0.6	0.00	0.00	-	0.885	-	0.000	0.0000	0.0000

ABRASIVE

MASK WIDTH

No	dn inch	is inch	dh inch	p ksi	type	size	m lb/min	valve setting	Vt in/mi	N rps	inc i/da	i inch	u in/mi	sp cn/sec	Np-cc pass	Np-c pass	sod inch	before grams	after grams	loss grams	area inch2	volume inch3 / KERF WIDT TOP	av. h inch	h/pss inch / KERF WIDTH BOTTOM	vol rate inch3/min / DELTA WIDTH
ISO PATTERN WITH USED MASK																									
57	5.047	3	0.018	50	gs	100	1.30	4.50	8000	10.96	0.6	0.028	6.18	8241	90	0	0.6	0.00	0.00	-	0.885	-	0.203	0.0023	0.5089
58	0.047	3	0.018	50	gs	100	1.30	4.50	8000	10.96	0.6	0.028	6.18	8241	10	0	0.6	0.00	0.00	-	0.885	-	0.023	0.0023	0.5189
DEEP KERF TESTS																									
EFFECT OF OVERLAP																									
59	0.062	3	0.018	50	gs	100	0.53	3.25	3806	15.92	0.6	0.037	35.54	47389	1	0	0.5	0.00	0.00	0.50	1.046	-	0.003	0.0030	0.05
60	0.062	3	0.018	50	gs	100	0.16	2.00	2000	10.62	0.1	0.006	3.95	5265	2	0	0.5	0.00	0.00	0.28	0.664	-	0.077	0.0385	0.04
61	0.062	3	0.018	50	gs	100	0.16	2.00	2000	10.62	0.3	0.019	11.85	15796	4	0	0.5	0.00	0.00	0.28	0.664	-	0.036	0.0090	0.03
62	0.062	3	0.018	50	gs	100	0.16	2.00	2000	10.62	0.6	0.037	23.69	31592	8	0	0.5	0.00	0.00	0.28	0.664	-	0.040	0.0050	0.03
63	0.062	3	0.018	50	gs	100	0.16	2.00	2000	10.62	0.9	0.056	35.54	47389	12	0	0.5	0.00	0.00	0.28	0.664	-	0.038	0.0032	0.03
64	0.062	5	0.018	50	gs	100	0.16	2.00	2000	10.62	1.2	0.074	47.39	63185	18	0	0.5	0.00	0.00	0.28	0.664	-	0.043	0.0024	0.03
THRU CUTTING ALUM -.250																									
EFFECT OF SPEED ON KERF WIDTH																									
65	0.047	4	0.018	50	gs	80	1.52	4.50	N/A	N/A	N/A	N/A	30.00	N/A	1	0	0.125	N/A	N/A	N/A	N/A	0.051		0.0370	0.014
66	0.047	4	0.018	50	gs	80	1.52	4.50	N/A	N/A	N/A	N/A	25.00	N/A	1	0	0.125	N/A	N/A	N/A	N/A	0.052		0.0380	0.014
67	0.047	4	0.018	50	gs	80	1.52	4.50	N/A	N/A	N/A	N/A	20.00	N/A	1	0	0.125	N/A	N/A	N/A	N/A	0.052		0.0400	0.012
68	0.047	4	0.018	50	gs	80	1.52	4.50	N/A	N/A	N/A	N/A	15.00	N/A	1	0	0.125	N/A	N/A	N/A	N/A	0.052		0.0430	0.009
69	0.047	4	0.018	50	gs	80	1.52	4.50	N/A	N/A	N/A	N/A	10.00	N/A	1	0	0.125	N/A	N/A	N/A	N/A	0.052		0.0450	0.007
70	0.047	4	0.018	50	gs	80	1.52	4.50	N/A	N/A	N/A	N/A	5.00	N/A	1	0	0.135	N/A	N/A	N/A	N/A	0.055		0.0490	0.006
THRU CUTTING STEEL -.250																									
EFFECT OF SPEED ON KERF WIDTH																									
71	0.047	4	0.018	50	gs	80	1.52	4.50	N/A	N/A	N/A	N/A	10.00	N/A	1	0	0.125	N/A	N/A	N/A	N/A	0.050		0.0360	0.014
72	0.047	4	0.018	50	gs	80	1.52	4.50	N/A	N/A	N/A	N/A	8.00	N/A	1	0	0.125	N/A	N/A	N/A	N/A	0.052		0.0380	0.014
73	0.047	4	0.018	52	gs	80	1.52	4.50	N/A	N/A	N/A	N/A	6.00	N/A	1	0	0.125	N/A	N/A	N/A	N/A	0.052		0.0400	0.012
74	0.047	4	0.018	50	gs	80	1.52	4.50	N/A	N/A	N/A	N/A	4.00	N/A	1	0	0.125	N/A	N/A	N/A	N/A	0.052		0.0430	0.009
75	0.047	4	0.018	50	gs	80	1.52	4.50	N/A	N/A	N/A	N/A	2.00	N/A	1	0	0.125	N/A	N/A	N/A	N/A	0.053		0.0460	0.007
76	0.047	4	0.018	50	gs	80	1.52	4.59	N/A	N/A	N/A	N/A	1.00	N/A	1	0	0.125	N/A	N/A	N/A	N/A	0.055		0.0500	0.005